Acoustic Scattering Cross Sections of Smart Obstacles: A Case Study

Lorella Fatone[1], Maria Cristina Recchioni[2] and Francesco Zirilli[3,*]

[1] *Dipartimento di Matematica e Informatica, Universitàdi Camerino, Via Madonna delle Carceri 9, 62032 Camerino (MC), Italy.*
[2] *Dipartimento di Scienze Sociali "D. Serrani", Università Politecnica delle Marche, Piazza Martelli 8, 60121 Ancona, Italy.*
[3] *CERI-Centro di Ricerca "Previsione Prevenzione e Controllo dei Rischi Geologici", Università di Roma "La Sapienza", Piazza Umberto Pilozzi 9, 00038 Valmontone (RM), Italy.*

Abstract. Acoustic scattering cross sections of smart furtive obstacles are studied and discussed. A smart furtive obstacle is an obstacle that, when hit by an incoming field, avoids detection through the use of a pressure current acting on its boundary. A highly parallelizable algorithm for computing the acoustic scattering cross section of smart obstacles is developed. As a case study, this algorithm is applied to the (acoustic) scattering cross section of a "smart" (furtive) simplified version of the NASA space shuttle when hit by incoming time-harmonic plane waves, the wavelengths of which are small compared to the characteristic dimensions of the shuttle. The solution to this numerically challenging scattering problem requires the solution of systems of linear equations with many unknowns and equations. Due to the sparsity of these systems of equations, they can be stored and solved using affordable computing resources. A cross section analysis of the simplified NASA space shuttle highlights three findings: i) the smart furtive obstacle reduces the magnitude of its cross section compared to the cross section of a corresponding "passive" obstacle; ii) several wave propagation directions fail to satisfactorily respond to the smart strategy of the obstacle; iii) satisfactory furtive effects along all directions may only be obtained by using a pressure current of considerable magnitude. Numerical experiments and virtual reality applications can be found at the website: `http://www.ceri.uniroma1.it/ceri/zirilli/w7`.

---

*Corresponding author. *Email addresses:* `lorella.fatone@unicam.it` (L. Fatone), `m.c.recchioni@univpm.it` (M. C. Recchioni), `f.zirilli@caspur.it` (F. Zirilli)

1   Introduction

A smart obstacle is an obstacle that, when hit by an incoming acoustic wave, responds by circulating a pressure current on its boundary according to the goals of the object's designed detection strategy. The pressure current is a quantity with physical dimensions of pressure divided by time. The most general class of smart obstacles considered by the authors (ghost obstacles) are obstacles that, when hit by an incoming wave, attempt to produce a scattered acoustic field that would be expected from a virtual obstacle (ghost) present under the same circumstances. The virtual object is designed to differ from the smart obstacle in both shape and position in space [5, 11]. This general class of smart obstacles includes, as special cases, furtive obstacles and masked obstacles. Furtive obstacles try to avoid detection when hit by an incoming wave by scattering a small amplitude wave [13]. When hit by an incoming wave, masked obstacles try to avoid detection by scattering an acoustic field that would be produced under the same circumstances by a virtual obstacle (a mask) that is different from the masked object in shape [9, 10]. Passive obstacles are obstacles that, when hit by an incoming acoustic field, do not respond by circulating a pressure current on their boundary as a way of manipulating their scattered field. Models of "smart obstacles" and scattering phenomena, introduced in [5, 9–11, 13, 15], are expressed as optimization (or optimal control) problems and partial differential equations. Some attempts at solving the time-harmonic inverse acoustic scattering problems associated with the inversion of these models by smart obstacles are described in [7, 8]. The mathematical model for the time-dependent scattering problem stated above, which is a generalization of the model considered here, is an optimal control problem for the wave equation [9, 11, 13]. Recently, physical examples of smart objects, such as phase-switched screens, have been designed and built (see, for example, [1–4]). Phase-switched screens are used to build radar absorbers and are an example in the electromagnetic domain of a smart object that pursues the goal of being furtive. In this paper, we develop a parallel numerical method for computing the acoustic scattering cross section of realistic smart obstacles. We use this algorithm to study the acoustic scattering cross section of smart furtive obstacles and compare the cross section with the scattering cross section of passive obstacles, that is, we study the furtivity effect. Cross sections of realistic smart obstacles at the wavelengths considered here have not been studied previously using mathematical models based on partial differential equations that describe the full wave propagation phenomenon. The behavior of these cross sections is relevant to understanding the impact of the smart strategies (i.e., the pressure currents used) on the fields scattered, and to the study of the relation between the geometry of the obstacles and the properties of the corresponding cross sections. Let $\mathbb{R}^3$ be three-dimensional real Euclidean space. To compute the cross section of a smart obstacle, we must solve the corresponding smart furtive obstacle scattering problem several times, which can be stated as follows: *given an incoming time-harmonic acoustic field propagating in $\mathbb{R}^3$ and a bounded obstacle $\Omega \subset \mathbb{R}^3$, which is non-empty and characterized by a nonnegative acoustic boundary impedance χ, find a time-harmonic pressure current circulating on the boundary of Ω*

that makes the field scattered by Ω, when hit by an incoming acoustic field, and the time-harmonic pressure current itself, "as small as possible".

This problem is formulated as a constrained optimization problem in an infinite dimensional space with the constraints given by an exterior boundary value problem for the Helmholtz equation (see Section 2, problems (2.5), (2.2a), (2.2b), and (2.4)). The spatial part of the time-harmonic pressure current is the independent variable of this optimization problem. Using the Lagrange multiplier method, the solution to the constrained optimization problem is translated into a solution to the first-order necessary optimality condition for the Lagrangian functional associated with the optimization problem. This first-order optimality condition can be expressed as an exterior problem for a system of two Helmholtz equations (see Section 2 problems (2.7a)-(2.7d)). By applying several assumptions along with a perturbation expansion known as the operator expansion method (see, for example, [13]), we reduce the solution to the exterior problem of this system of Helmholtz equations to a solution of a sequence of nested systems of first kind integral equations (see Section 3, Eqs. (3.7a), and (3.7b)). Furthermore, using a suitable wavelet basis to represent the kernels, unknowns, and data of these systems of integral equations, we approximate the system of equations as a set of sparse systems of linear equations (see Section 4 formula (3.14)). To exploit the sparsity and structure of these linear systems, we developed an ad hoc parallel solver based on the conjugate gradient method. Because these integrals are independent one of another, we used parallel computing to evaluate the four- and two-dimensional integrals that define the entries of the coefficient matrix and to calculate the right hand side of the linear systems.

Moreover, because the cross section analysis presented requires knowledge of the solid angles of the far field patterns relative to several tens of incoming waves, we numerically solved, in parallel, tens of time-harmonic smart scattering problems. To do so, we divided the processors at our disposal into groups and devoted each group of processors to the computation of a subset of these time-harmonic problems. The above-described numerical methods for evaluating the (acoustic) scattered fields and scattering cross section (see Section 2 formula (2.12)) generated by an obstacle were executed on the IBM Power6 Supercomputer Huygens of the SARA Computing & Networking Service (Amsterdam and Almere-The Netherlands). The total number of cores of the supercomputer is 3328, with a peak performance for the full configuration of 60 TeraFlop/s. The numerical results reported here were obtained using 300,000 CPU time hours and (at most) 512 cores made available to us on the SARA Huygens machine through the research contract "AEMCSSO-Acoustic and ElectroMagnetic Cross Sections of Smart Obstacles" granted to CERI-Università di Roma "La Sapienza" by the European Union in its FPG-Research Infrastructure Project (EU FP6 project RI-031513 and the FP7 project RI-222919). The contract AEMCSSO belongs to the 2007 Extreme Computing Initiative sponsored by DEISA (Distributed European Infrastructure for Supercomputing Applications, www.deisa.eu).

Our numerical experiments resulted in three main findings. First, the magnitude of the cross section of a passive obstacle is larger than the magnitude of the corresponding cross section of a smart (furtive) obstacle. Second, some elements of the obstacle are more

difficult to hide in a cross section than others. It will be useful to focus on scattering from these elements via the smart behavior enforcement induced by the pressure current used. Third, to make an obstacle undetectable in all directions, pressure currents of considerable size are required. Numerical experiments and virtual reality applications, including stereographic applications that show the acoustic scattering cross section of a simplified NASA space shuttle, can be found at the website: `http://www.ceri.uniroma1.it/ceri/zirilli/w7`. For an overview of the issues associated with acoustic and electromagnetic scattering, the reader is referred to the general references provided by the authors on the website: `http://www.econ.univpm.it/recchioni/scattering`.

The paper is organized as follows. In Section 2, we present the mathematical model used here to describe smart obstacles. This model implicitly defines the field scattered by a smart obstacle and the corresponding cross section. In Section 3, we approximate the solution to Eqs. (2.7a)-(2.7d) using the solution to a set of systems of linear equations using appropriate wavelet bases, and we discuss how to numerically solve these systems of linear equations. Moreover, we show how to evaluate, in parallel, the (acoustic) scattering cross sections. In Section 4, we describe the parallel implementation of the computational method presented in Section 3. In Section 5, we present the numerical results obtained from computation of the acoustic scattering cross section of a furtive simplified model of the NASA space shuttle (Fig. 1(a)) as a function of the smart strategy.
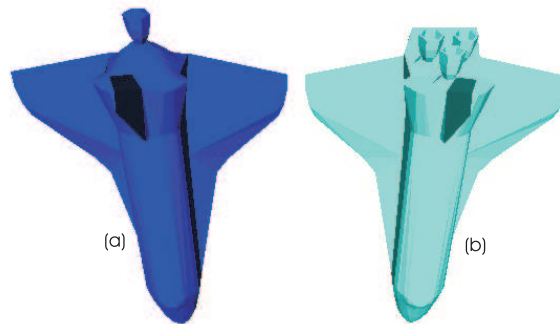

Figure 1: (a) Simplified NASA space shuttle, (b) NASA space shuttle.

2   The mathematical model of a smart obstacle

Let us formulate the mathematical model used to study the time-harmonic scattering problem involving smart furtive obstacles stated in Section 1. Let r be a positive integer, $\mathbb{R}$ be the set of real numbers, and $\mathbb{R}^r$ be the r-dimensional real Euclidean space. For convenience, let $\mathbb{C}$, $\mathbb{C}^r$ be the set of complex numbers and the r-dimensional complex Euclidean space, respectively.

Let $\Omega \subset \mathbb{R}^3$ be a (nonempty) bounded simply connected open set, the boundary $\partial\Omega$ of which is a locally Lipschitz surface characterized by a nonnegative constant acoustic

boundary impedance χ. Without loss of generality, we assume that Ω contains the origin. We denote by $\underline{n}(\underline{x}) = (n_1(\underline{x}), n_2(\underline{x}), n_3(\underline{x}))^T \in \mathbb{R}^3$, the outward unit normal vector to $\partial\Omega$ in $\underline{x} \in \partial\Omega$. Since Ω has a locally Lipschitz boundary, the vector $\underline{n}(\underline{x})$, $\underline{x} \in \partial\Omega$ exists almost everywhere in $\partial\Omega$ (see [13] and the references therein). We denote by $\overline{\Omega}$ the closure of Ω. The couple $(\Omega; \chi)$ may sometimes be called the obstacle. We assume that $(\Omega; \chi)$ is immersed in a homogeneous isotropic medium at rest, which fills $\mathbb{R}^3 \setminus \Omega$ with no source terms present. Let $(\cdot, +)$ be the Euclidean scalar product in $\mathbb{R}^3$, and let $\|\cdot\|$ be the induced vector norm in $\mathbb{R}^3$, where $\cdot$, $+$ denote generic vectors in $\mathbb{R}^3$. We consider an acoustic incoming time-harmonic plane wave $u^i(\underline{x}, t)$, $(\underline{x}, t) \in \mathbb{R}^3 \times \mathbb{R}$, propagating in the medium with velocity $c > 0$, with frequency $\omega \neq 0$, and with space-dependent part $u^i_{k,\underline{\alpha}}$. That is,

$$u^i(\underline{x}, t) = e^{-\iota\omega t} u^i_{k,\underline{\alpha}}(\underline{x}) = e^{-\iota\omega t} e^{\iota k(\underline{x}, \underline{\alpha})}, \qquad (\underline{x}, t) \in \mathbb{R}^3 \times \mathbb{R}, \tag{2.1}$$

where ι is the imaginary unit, $k = \omega/c$ is the wave number, $\underline{\alpha} \in \mathbb{R}^3$ is a unit vector that indicates the propagation direction of the wave (2.1). Let us denote by $u^s_{k,\underline{\alpha}}(\underline{x})$, $\underline{x} \in \mathbb{R}^3 \setminus \overline{\Omega}$, the space-dependent part of the time-harmonic field scattered by the smart obstacle $(\Omega; \chi)$ when hit by an incoming wave u^i given by (2.1), if $\psi(\underline{x}, t)$ is the time-harmonic pressure current acting on $\partial\Omega$ as the response to the incoming wave. That is, let $\psi(\underline{x}, t) = ce^{-\iota\omega t} \psi_{k,\underline{\alpha}}(\underline{x})$, $(\underline{x}, t) \in \partial\Omega \times \mathbb{R}$, where $c\psi_{k,\underline{\alpha}}$ is the space-dependent part of the pressure current. Note that the wave propagation velocity c appears in the definition of the spatial part of $\psi(\underline{x}, t)$, which simplifies some of the formulae derived later. The scattered field $u^s_{k,\underline{\alpha}}(\underline{x})$, $\underline{x} \in \mathbb{R}^3 \setminus \overline{\Omega}$, is the solution to the following boundary value problem for the Helmholtz equation (see [13]):

$$\left(\triangle u^s_{k,\underline{\alpha}} + k^2 u^s_{k,\underline{\alpha}} \right)(\underline{x}) = 0, \qquad\qquad \underline{x} \in \mathbb{R}^3 \setminus \overline{\Omega}, \tag{2.2a}$$

$$\iota k u^s_{k,\underline{\alpha}}(\underline{x}) + \chi \frac{\partial u^s_{k,\underline{\alpha}}}{\partial \underline{n}(\underline{x})}(\underline{x}) = (1+\chi)\psi_{k,\underline{\alpha}}(\underline{x}) + b_{k,\underline{\alpha}}(\underline{x}), \qquad \underline{x} \in \partial\Omega, \tag{2.2b}$$

where $b_{k,\underline{\alpha}}$ is given by

$$b_{k,\underline{\alpha}}(\underline{x}) = -\iota k e^{\iota k(\underline{x}, \underline{\alpha})} \left(1 + \chi(\underline{n}(\underline{x}), \underline{\alpha}) \right), \qquad \underline{x} \in \partial\Omega, \tag{2.3}$$

with the Sommerfeld radiation condition at infinity

$$\frac{\partial u^s_{k,\underline{\alpha}}(\underline{x})}{\partial r} - \iota k u^s_{k,\underline{\alpha}}(\underline{x}) = o\left(\frac{1}{r}\right), \qquad r \to +\infty, \tag{2.4}$$

where $\Delta = \sum_{i=1}^3 \partial^2/\partial x_i^2$ is the Laplace operator, $r = \|\underline{x}\|$, $\underline{x} \in \mathbb{R}^3$, and $o(\cdot)$ and $\mathcal{O}(\cdot)$ are the Landau symbols. Note that the factor $(1+\chi)$ in front of $\psi_{k,\underline{\alpha}}(\underline{x})$, $\underline{x} \in \partial\Omega$, in (2.2b) was introduced to simplify some of the formulae derived below. Let us point out that the function $c\psi_{k,\underline{\alpha}}(\underline{x})$, $\underline{x} \in \partial\Omega$, can be seen as the space-dependent part of the control function of the optimal control problem for the wave equation used to model the time-dependent acoustic scattering problem, which generalizes problems (2.2a)-(2.4) (see [13]).

Note that when we choose $\psi_{k,\underline{\alpha}}(\underline{x}) = 0$, $\underline{x} \in \partial\Omega$, in (2.2b), problems (2.2a)-(2.4) becomes the acoustic time-harmonic scattering problem for a passive obstacle $(\Omega; \chi)$. The smart (furtive) obstacle scattering problem described in Section 1 is translated into the following constrained optimization problem:

$$\min_{\psi_{k,\underline{\alpha}} \in C} L_{k,\underline{\alpha},\lambda,\mu}(\psi_{k,\underline{\alpha}}), \tag{2.5}$$

subject to the constraints (2.2a), (2.2b), (2.4), where the cost functional $L_{k,\underline{\alpha},\lambda,\mu}$ is given by

$$L_{k,\underline{\alpha},\lambda,\mu}(\psi_{k,\underline{\alpha}}) = \int_{\partial\Omega} ds_{\partial\Omega}(\underline{x})(1+\chi)\left[\lambda|u_{k,\underline{\alpha}}^s(\underline{x})|^2 + \mu\varsigma|\psi_{k,\underline{\alpha}}(\underline{x})|^2\right], \quad \psi_{k,\underline{\alpha}} \in C, \tag{2.6}$$

$ds_{\partial\Omega}$ is the surface measure on $\partial\Omega$, $\lambda \geq 0$ and $\mu \geq 0$ are adimensional constants such that $\lambda + \mu = 1$, ς is a positive dimensional constant that, without loss of generality, we can assume to be one, C is a suitable set of admissible functions that, for simplicity, we leave unspecified here (see [5] for further details), and $|\cdot|$ is the norm of $\cdot$ in $\mathbb{C}$. The function $\psi_{k,\underline{\alpha}}$ is the independent variable of the constrained optimization problems (2.5), (2.2a), (2.2b), (2.4). The case $\chi = +\infty$, which is the case of acoustically hard obstacles, can be treated with some modifications to the Eqs. (2.2a)-(2.4), which are omitted to maintain the simplicity of this exposition. Note that the simplified NASA space shuttle studied in Section 5 is modeled as an acoustically hard obstacle. Given (2.6), it is easy to see that when $\mu = 0$ or $\mu = 1$, problems (2.5), (2.2a), (2.2b), (2.4) is trivial, see [5, 13]. The choice of the cost functional (2.6) is motivated by the fact that when $0 < \mu < 1$, we have $\lambda > 0$, that is, when $0 < \mu < 1$, the minimization of $L_{k,\underline{\alpha},\lambda,\mu}$ minimizes the field scattered by the smart obstacle and the corresponding pressure current on $\partial\Omega$. As a consequence, the scattered field on $\mathbb{R}^3 \setminus \overline{\Omega}$ is also minimized. That is, the function $\psi_{k,\underline{\alpha}}$, which is a solution to (2.5), (2.2a), (2.2b), (2.4) for the cost functional given by (2.6), $0 < \mu < 1$, makes an obstacle $(\Omega; \chi)$ furtive when it is hit by an incoming wave (2.1). Let $\varphi_{k,\underline{\alpha}}(\underline{x})$, $\underline{x} \in \mathbb{R}^3 \setminus \overline{\Omega}$, be the Lagrange multiplier of the constrained optimization problems (2.5), (2.2a), (2.2b), (2.4). Under some assumptions on the admissible functions $\psi_{k,\underline{\alpha}}(\underline{x})$, $\underline{x} \in \partial\Omega$, and on the auxiliary functions $\varphi_{k,\underline{\alpha}}(\underline{x})$, $\underline{x} \in \mathbb{R}^3 \setminus \overline{\Omega}$, the first-order optimality condition for the Lagrangian functional associated with the constrained optimization problems (2.5), (2.2a), (2.2b), (2.4), can be written as follows (see [5, 13]):

$$\left(\triangle u_{k,\underline{\alpha}}^s + k^2 u_{k,\underline{\alpha}}^s\right)(\underline{x}) = 0, \qquad \left(\triangle \varphi_{k,\underline{\alpha}} + k^2 \varphi_{k,\underline{\alpha}}\right)(\underline{x}) = 0, \qquad \underline{x} \in \mathbb{R}^3 \setminus \overline{\Omega}, \tag{2.7a}$$

$$\imath k u_{k,\underline{\alpha}}^s(\underline{x}) + \chi \frac{\partial u_{k,\underline{\alpha}}^s}{\partial \underline{n}(\underline{x})}(\underline{x}) + \frac{(1+\chi)}{\varsigma}\varphi_{k,\underline{\alpha}}(\underline{x}) = b_{k,\underline{\alpha}}(\underline{x}), \qquad \underline{x} \in \partial\Omega, \tag{2.7b}$$

$$\imath k \mu \varphi_{k,\underline{\alpha}}(\underline{x}) - \mu\chi \frac{\partial \varphi_{k,\underline{\alpha}}}{\partial \underline{n}(\underline{x})}(\underline{x}) = -\lambda(1+\chi)u_{k,\underline{\alpha}}^s(\underline{x}), \qquad \underline{x} \in \partial\Omega, \tag{2.7c}$$

$$\frac{\partial u_{k,\underline{\alpha}}^s(\underline{x})}{\partial r} - \imath k u_{k,\underline{\alpha}}^s(\underline{x}) = o\left(\frac{1}{r}\right), \qquad \frac{\partial \varphi_{k,\underline{\alpha}}(\underline{x})}{\partial r} + \imath k \varphi_{k,\underline{\alpha}}(\underline{x}) = o\left(\frac{1}{r}\right), \qquad r \to +\infty, \tag{2.7d}$$

where $b_{k,\underline{\alpha}}$ is given by (2.3). Problems (2.7a)-(2.7d) is an exterior boundary value problem in the two unknowns $u_{k,\underline{\alpha}}$, $\varphi_{k,\underline{\alpha}}$ for a system of Helmholtz equations (2.7a) coupled

through the boundary conditions (2.7b), (2.7c), and with the boundary conditions at infinity (2.7d). The relation between $\varphi_{k,\underline{\alpha}}$, the solution to the problems (2.7a)-(2.7d), and the function $\psi_{k,\underline{\alpha}} = \widehat{\psi}_{k,\underline{\alpha}}$, the solution to the problems (2.5), (2.2a), (2.2b), (2.4), is (see [6, 13]):

$$\psi_{k,\underline{\alpha}}(\underline{x}) = \widehat{\psi}_{k,\underline{\alpha}}(\underline{x}) = -\frac{1}{\varsigma}\varphi_{k,\underline{\alpha}}(\underline{x}), \qquad \underline{x} \in \partial\Omega. \tag{2.8}$$

Under the hypotheses used to deduce (2.7a)-(2.7d), we can say that the problems (2.7a)-(2.7d) and the condition (2.8) are a formulation of the time-harmonic furtive obstacle scattering problem in the form of a system of partial differential equations, which is equivalent to the original formulation (2.5), (2.2a), (2.2b), (2.4), (2.6) as a constrained optimization problem. Let $B = \{\underline{x} \in \mathbb{R}^3 | \|\underline{x}\| < 1\}$, ∂B be the boundary of B, and let $F^0_{\lambda,\mu}(\hat{\underline{x}}, k, \underline{\alpha})$, $\hat{\underline{x}}$, $\underline{\alpha} \in \partial B$, $k = \omega/c \in \mathbb{R}$, be the far field associated with $u^s_{k,\underline{\alpha}}(\underline{x})$, the solution to (2.5), (2.2a), (2.2b), (2.4). We have,

$$u^s_{k,\underline{\alpha}}(\underline{x}) = \frac{e^{ikr}}{r}F^0_{\lambda,\mu}(\hat{\underline{x}}, k, \underline{\alpha}) + \mathcal{O}\left(\frac{1}{r^2}\right), \quad \underline{x} = r\hat{\underline{x}} \in \mathbb{R}^3 \setminus \overline{\Omega}, \quad r \to +\infty. \tag{2.9}$$

Note that, in general, $F^0_{\lambda,\mu}(\hat{\underline{x}}, k, \underline{\alpha})$, $k \in \mathbb{R}$, $\hat{\underline{x}}, \underline{\alpha} \in \partial B$, is a complex function of its arguments. The acoustic cross section $C_{\lambda,\mu}(\hat{\underline{x}}, k)$, $\hat{\underline{x}} \in \partial B$, $k \in \mathbb{R}$, of $(\Omega; \chi)$ associated with the scattering phenomenon described previously is defined as follows:

$$C_{\lambda,\mu}(\hat{\underline{x}}, k) = \int_{\partial B}|F^0_{\lambda,\mu}(\hat{\underline{x}}, k, \underline{\alpha})|^2 ds_{\partial B}(\underline{\alpha}), \quad \hat{\underline{x}} \in \partial B, \quad k \in \mathbb{R}, \tag{2.10}$$

where $ds_{\partial B}$ is the surface measure on ∂B. Note that in (2.9) and (2.10), we have chosen to keep the notation simple by omitting the dependence of $F^0_{\lambda,\mu}$ and of $C_{\lambda,\mu}$ from ς. Let N_θ, N_ϕ, M_θ, and M_ϕ be positive integers greater than one, and let S_{N_θ,N_ϕ}, $I_{M_\theta,M_\phi} \subset \partial B$ be the following sets:

$$S_{N_\theta,N_\phi} = \left\{\hat{\underline{x}}_{i,j} = \left(\sin\theta^N_i\cos\phi^N_j, \sin\theta^N_i\sin\phi^N_j, \cos\theta^N_i\right)^T, \ \theta^N_i = i\frac{\pi}{N_\theta - 1},\right.$$

$$\phi^N_j = j\frac{2\pi}{N_\phi}, \ i = 1,2,\cdots,N_\theta - 2, \ j = 0,1,\cdots,N_\phi - 1\bigg\} \cup$$

$$\left\{\hat{\underline{x}}_{i,i} = (0,0,\cos\theta^N_i)^T, \ \theta^N_i = i\frac{\pi}{N_\theta - 1}, \ i = 0, N_\theta - 1\right\}, \tag{2.11a}$$

$$I_{M_\theta,M_\phi} = \left\{\underline{\alpha}_{i,j} = \left(\sin\theta^M_i\cos\phi^M_j, \sin\theta^M_i\sin\phi^M_j, \cos\theta^M_i\right)^T, \ \theta^M_i = i\frac{\pi}{M_\theta - 1},\right.$$

$$\phi^M_j = j\frac{2\pi}{M_\phi}, \ i = 1,2,\cdots,M_\theta - 2, \ j = 0,1,\cdots,M_\phi - 1\bigg\} \cup$$

$$\left\{\underline{\alpha}_{i,i} = (0,0,\cos\theta^M_i)^T, \ \theta^M_i = i\frac{\pi}{M_\theta - 1}, \ i = 0, M_\theta - 1\right\}. \tag{2.11b}$$

Given $k \in \mathbb{R}$ and $k \neq 0$, the acoustic scattering cross section $C_{\lambda,\mu}(\hat{\underline{x}}, k)$, $\hat{\underline{x}} \in \partial B$ is evaluated by approximating the integral appearing in (2.10) using the rectangular quadrature rule

applied to the set of nodes given by I_{M_θ,M_ϕ}. Considering that S_{N_θ,N_ϕ} defines a set of observation directions, $C_{\lambda,\mu}(\underline{\hat{x}},k)$, $\underline{\hat{x}} \in \partial B$ is approximated by:

$$\tilde{C}_{\lambda,\mu}(\underline{\hat{x}},k) = \sum_{i=1}^{M_\theta-2} \sin(\theta_i^M) \sum_{j=0}^{M_\phi-1} |F_{\lambda,\mu}^0(\underline{\hat{x}},k,\underline{\alpha}_{i,j})|^2, \qquad \underline{\hat{x}} \in S_{N_\theta,N_\phi} \subset \partial B. \qquad (2.12)$$

To evaluate $\tilde{C}_{\lambda,\mu}(\underline{\hat{x}},k)$ defined in (2.12), for $\underline{\hat{x}} \in S_{N_\theta,N_\phi}$, we must solve $(M_\theta-2)\cdot M_\phi$ and the time-harmonic scattering problems (2.7a)-(2.7d) in order to obtain the corresponding far fields. These problems are independent of each other and can be solved in parallel. Parallel computing makes possible the study of the case presented in Section 5, with reasonable effort. Identifying a solution to this realistic problem enables an understanding of how smart effects on the far fields, induced by the function $\psi_{k,\underline{\alpha}}(\underline{x})$, $\underline{x} \in \partial\Omega$, change with the propagation direction of the incoming plane wave (i.e., with $\underline{\alpha} \in \partial B$) and with the perspective of the observer (i.e., with the vector $\underline{\hat{x}} \in \partial B$ of $F_{\lambda,\mu}^0(\underline{\hat{x}},k,\underline{\alpha})$). The smart effects on the far fields are additionally reflected in the acoustic cross section.

3 Solution to the exterior problem and computation of the cross section

Let (x_1,x_2,x_3) be the canonical Cartesian coordinates of $\mathbb{R}^3$. We consider a cylindrical coordinate system that has x_3 as the cylindrical axis given by (r_1,ϕ,x_3), where $r_1 = \sqrt{x_1^2 + x_2^2}$ and $\phi = \arctan(x_2/x_1)$, x_1, $x_2 \in \mathbb{R}$. Some attention must be paid in the use of these formulae for $x_1 = 0$. To solve the exterior problems (2.7a)-(2.7d), we use the operator expansion method expressed in the cylindrical coordinate system defined above. This choice is motivated by the shape of the obstacle studied in the numerical experiments presented in Section 5 (see Fig. 1(a)). Let us summarize the operator expansion method used to approximate the exterior problem (2.7a)-(2.7d) using a set of sparse linear systems, which must be solved numerically. For $(k,\underline{\alpha}) \in \mathbb{R} \times \partial B$, $k \neq 0$, we assume that

(a) the boundary of the obstacle $\partial\Omega$ can be represented as follows:

$$\partial\Omega = \left\{ \underline{x} = (r_1\cos\phi, r_1\sin\phi, x_3)^T \in \mathbb{R}^3 \,\middle|\, r_1 = \xi(\phi,x_3), \ \phi \in [0,2\pi), \ x_3 \in [x_{3,i},x_{3,f}] \right\}, \quad (3.1)$$

where $x_{3,i}$, $x_{3,f}$ are real numbers such that $x_{3,i} < x_{3,f}$ and $\xi(\phi,x_3) \geq 0$, $\phi \in [0,2\pi)$, $x_3 \in [x_{3,i},x_{3,f}]$, is a single valued function that we assume is sufficiently regular that the following formulae may be defined. Moreover, we assume that $\xi(\phi,x_3) > 0$, $\phi \in [0,2\pi]$, $x_3 \in (x_{3,i},x_{3,f})$. When Eq. (3.1) holds, it is easy to see that there exists a bounded simply connected open set $\Omega_c \subset \Omega$ with a locally Lipschitz boundary $\partial\Omega_c \subset \Omega$ such that $\partial\Omega_c$ can be represented as

$$\partial\Omega_c = \left\{ \underline{x} = (r_1\cos\phi, r_1\sin\phi, x_3)^T \in \mathbb{R}^3 \,\middle|\, r_1 = \xi_c(\phi,x_3), \ \phi \in [0,2\pi), \ x_3 \in [\tilde{x}_{3,i},\tilde{x}_{3,f}] \right\}, \quad (3.2)$$

where $\tilde{x}_{3,i}$, $\tilde{x}_{3,f}$ are real numbers such that $\tilde{x}_{3,i} < \tilde{x}_{3,f}$, $[\tilde{x}_{3,i},\tilde{x}_{3,f}] \subset (x_{3,i},x_{3,f})$ and $\xi_c(\phi,x_3) \geq 0$, $\phi \in [0,2\pi), x_3 \in [\tilde{x}_{3,i},\tilde{x}_{3,f}]$ is a single valued function that is sufficiently regular that the following formulae may be defined. We assume that $\xi_c(\phi,x_3) > 0$, $\phi \in [0,2\pi]$, $x_3 \in (\tilde{x}_{3,i},\tilde{x}_{3,f})$. Moreover, there exists a surface measure $ds_{\partial\Omega_c}$, defined on $\partial\Omega_c$, given by

$$ds_{\partial\Omega_c}\left(\underline{x}(\phi,x_3)\right) = g_c(\phi,x_3)d\phi dx_3, \qquad (\phi,x_3) \in U', \qquad (3.3)$$

where $U' = (0,2\pi) \times (\tilde{x}_{3,i},\tilde{x}_{3,f})$, $d\phi dx_3$ is the usual Lebesgue measure on U', and g_c is an almost everywhere positive function defined on U';

(b) the functions $u^s_{k,\underline{\alpha}}$, $\varphi_{k,\underline{\alpha}}$, $\underline{\alpha} \in \partial B$, $k \in \mathbb{R}$, which are solutions to the exterior problems (2.7a)-(2.7d), can be represented as single layer acoustic potentials with density functions defined on $\partial\Omega_c$. That is, we assume that

$$u^s_{k,\underline{\alpha}}(\underline{x}) = \int_{U'} d\underline{v}' g_c(\underline{v}')\Phi_k(\underline{x},\underline{y}_{\underline{\xi}_c}(\underline{v}'))c_{k,\underline{\alpha}}(\underline{y}_{\underline{\xi}_c}(\underline{v}')), \quad \underline{\alpha} \in \partial B, \quad k \in \mathbb{R}, \qquad (3.4a)$$

$$\varphi_{k,\underline{\alpha}}(\underline{x}) = \int_{U'} d\underline{v}' g_c(\underline{v}')\overline{\Phi_k(\underline{x},\underline{y}_{\underline{\xi}_c}(\underline{v}'))}f_{k,\underline{\alpha}}(\underline{y}_{\underline{\xi}_c}(\underline{v}')), \quad \underline{\alpha} \in \partial B, \quad k \in \mathbb{R}, \qquad (3.4b)$$

where $\underline{y}_{\underline{\xi}_c}(\underline{v}') = (\xi_c(\underline{v}')\cos(\phi'),\xi_c(\underline{v}')\sin(\phi'), x'_3)^T$, $\underline{v}' = (\phi',x'_3)^T \in U'$ denotes a point belonging to $\partial\Omega_c$, $d\underline{v}' = d\phi' dx'_3$ is the Lebesgue measure on U',

$$\Phi_k(\underline{x},\underline{y}) = \frac{e^{ik\|\underline{x}-\underline{y}\|}}{4\pi\|\underline{x}-\underline{y}\|}, \qquad \underline{x},\underline{y} \in \mathbb{R}^3, \qquad \underline{x} \neq \underline{y},$$

is the fundamental solution to the Helmholtz operator on $\mathbb{R}^3$ satisfying the "radiation" condition (2.7d) at infinity, $\overline{\Phi}_k$ is the complex conjugate of Φ_k, and $c_{k,\underline{\alpha}}$, $f_{k,\underline{\alpha}}$ are the unknown density functions of the single layer acoustic potentials (3.4a), (3.4b) used to represent $u^s_{k,\underline{\alpha}}$ and $\varphi_{k,\underline{\alpha}}$, respectively, that we have assumed exist;

(c) there exists a surface $\partial\Omega_r$ with a boundary consisting of a simply connected open set Ω_r that can be represented by a formula analogous to formula (3.1) if we replace the function ξ with a suitable single valued function ξ_r. The surface $\partial\Omega_r$ will be called the reference surface. Note that we do not assume that $\partial\Omega_r \subset \Omega$. To guarantee convergence of the operator expansion method, it is convenient to choose $\partial\Omega_r$ such that the "distance" between $\partial\Omega_r$ and $\partial\Omega$ is small. The reference surface $\partial\Omega_r$ is usually a smoothed and simplified version of the surface $\partial\Omega$. We assume that the following expansions of the functions $u^s_{k,\underline{\alpha}}$, $\varphi_{k,\underline{\alpha}}$, defined in (3.4a), (3.4b), hold:

$$u^s_{k,\underline{\alpha}}(\underline{x}) = \int_{U'} d\underline{v}' g_c(\underline{v}')\Phi_k(\underline{x},\underline{y}_{\underline{\xi}_c}(\underline{v}'))c_{k,\underline{\alpha}}(\underline{y}_{\underline{\xi}_c}(\underline{v}'))$$

$$= \int_{U'} d\underline{v}' g_c(\underline{v}')\Phi_k(\underline{x},\underline{y}_{\underline{\xi}_c}(\underline{v}'))\sum_{s=0}^{+\infty} c_{k,\underline{\alpha},s}(\underline{v}'), \quad \underline{x} \in \mathbb{R}^3\backslash\Omega, \ \underline{\alpha} \in \partial B, \ k \in \mathbb{R}, \quad (3.5a)$$

$$\varphi_{k,\underline{\alpha}}(\underline{x}) = \int_{U'} d\underline{v}' g_c(\underline{v}') \overline{\Phi_k(\underline{x}, \underline{y}_{\underline{\xi}_c}(\underline{v}'))} f_{k,\underline{\alpha}}(\underline{y}_{\underline{\xi}_c}(\underline{v}'))$$

$$= \int_{U'} d\underline{v}' g_c(\underline{v}') \overline{\Phi_k(\underline{x}, \underline{y}_{\underline{\xi}_c}(\underline{v}'))} \sum_{s=0}^{+\infty} f_{k,\underline{\alpha},s}(\underline{v}'), \quad \underline{x} \in \mathbb{R}^3 \setminus \Omega, \ \underline{\alpha} \in \partial B, \ k \in \mathbb{R}, \quad (3.5b)$$

where $c_{k,\underline{\alpha},s} = \mathcal{O}((\xi - \xi_r)^s)$ for $\xi \to \xi_r$ or $c_{k,\underline{\alpha},s} = 0$, and $f_{k,\underline{\alpha},s} = \mathcal{O}((\xi - \xi_r)^s)$ for $\xi \to \xi_r$ or $f_{k,\underline{\alpha},s} = 0$, $s = 0,1,\cdots$.

Let $U = (0,2\pi) \times (x_{3,i}, x_{3,f})$, $\underline{x}_{\underline{\xi}}$ be a map from U to $\partial \Omega$, and $\underline{x}_{\underline{\xi}_r}$ be a map from U to $\partial \Omega_r$. The maps $\underline{x}_{\underline{\xi}}$, $\underline{x}_{\underline{\xi}_r}$ are defined analogously to the map $\underline{y}_{\underline{\xi}_c}$ from U' to $\partial \Omega_c$, introduced above. Moreover, let $\nabla_{\underline{x}}$ be the gradient operator with respect to $\underline{x} \in \mathbb{R}^3$, and let $\underline{\phi}_k(\underline{v}) = (1/\imath k) \chi \underline{n}(\underline{x}_{\underline{\xi}}(\underline{v}))$, $\underline{v} \in U$, $k \neq 0$. For $\nu = 0,1,\cdots$, we define

$$\underline{Q}^\nu(\underline{v},\underline{y}) = \frac{\partial^\nu}{\partial r_1^\nu} \nabla_{\underline{x}} \Phi_k \big((r_1 \cos\phi, r_1 \sin\phi, x_3)^T, \underline{y} \big) \big|_{r_1 = \xi_r(\underline{v})}, \quad \underline{v} \in U, \ \underline{y} \in \mathbb{R}^3 \setminus \partial \Omega_r, \quad (3.6a)$$

$$\mathcal{L}^\nu(\underline{v},\underline{y}) = \frac{\partial^\nu}{\partial r_1^\nu} \Phi_k \big((r_1 \cos\phi, r_1 \sin\phi, x_3)^T, \underline{y} \big) \big|_{r_1 = \xi_r(\underline{v})}, \quad \underline{v} \in U, \ \underline{y} \in \mathbb{R}^3 \setminus \partial \Omega_r. \quad (3.6b)$$

Using assumptions (a)-(c), substituting (3.5a), (3.5b) into the boundary conditions (2.7b), (2.7c), and arguing as in [6], we obtain a sequence of systems of integral equations that depend on the index s, $s = 0,1,\cdots$. The sequence contains one system for each order s in the expansion in powers of $(\xi - \xi_r)$ of the unknown density functions appearing in (3.5a), (3.5b). That is, at order s, we have (see [6])

$$\int_{U'} d\underline{v}' K_{\xi_r,\xi_c}(\underline{v},\underline{v}') c_{k,\underline{\alpha},s}(\underline{v}') + \frac{(1+\chi)}{2\varsigma kc} \int_{U'} d\underline{v}' \imath \overline{\Phi_k(\underline{x}_{\underline{\xi}_r}(\underline{v}), \underline{y}_{\underline{\xi}_c}(\underline{v}'))} f_{k,\underline{\alpha},s}(\underline{v}')$$

$$= d_{1,k,\underline{\alpha},s}(\underline{v}), \qquad \underline{v} \in U, \quad s = 0,1,2,\cdots, \tag{3.7a}$$

$$-\frac{2\lambda(1+\chi)}{kc} \int_{U'} d\underline{v}' \imath \Phi_k(\underline{x}_{\underline{\xi}_r}(\underline{v}), \underline{y}_{\underline{\xi}_c}(\underline{v}')) c_{k,\underline{\alpha},s}(\underline{v}') + \mu \int_{U'} d\underline{v}' \overline{K_{\xi_r,\xi_c}(\underline{v},\underline{v}')} f_{k,\underline{\alpha},s}(\underline{v}')$$

$$= d_{2,k,\alpha,s}(\underline{v}), \qquad \underline{v} \in U, \quad s = 0,1,2,\cdots, \tag{3.7b}$$

where K_{ξ_r,ξ_c} is given by

$$K_{\xi_r,\xi_c}(\underline{v},\underline{v}') = \Big[\Phi_k(\underline{x}_{\underline{\xi}_r}(\underline{v}), \underline{y}_{\underline{\xi}_c}(\underline{v}')) + \big(\underline{\phi}_k(\underline{v}), (\nabla_{\underline{x}} \Phi_k)(\underline{x}_{\underline{\xi}_r}(\underline{v}), \underline{y}_{\underline{\xi}_c}(\underline{v}')) \big) \Big], \quad \underline{v} \in U, \ \underline{v}' \in U', \tag{3.8}$$

and for $s = 0,1,\cdots$, the right hand sides $d_{j,k,\underline{\alpha},s}$, $j=1,2$, of the integral equations (3.7a), (3.7b) are given by

$$d_{1,k,\underline{\alpha},0}(\underline{v}) = -e^{\imath k (\underline{x}_{\underline{\xi}}(\underline{v}), \underline{\alpha})} \big[1 + \chi \big(\underline{n}(\underline{x}_{\underline{\xi}}(\underline{v})), \underline{\alpha} \big) \big], \quad d_{2,k,\underline{\alpha},0}(\underline{v}) = 0, \quad \underline{v} \in U, \tag{3.9a}$$

$$d_{1,k,\underline{\alpha},s}(\underline{v}) = -\sum_{\nu=0}^{s-1} \frac{(\xi(\underline{v}) - \xi_r(\underline{v}))^{s-\nu}}{(s-\nu)!} \int_{U'} d\underline{v}' \Big\{ \Big[\big(\underline{\phi}_k(\underline{v}), \underline{Q}^{s-\nu}(\underline{v}, \underline{y}_{\underline{\xi}_c}(\underline{v}')) \big) + \mathcal{L}^{s-\nu}(\underline{v}, \underline{y}_{\underline{\xi}_c}(\underline{v}')) \Big] c_{k,\underline{\alpha},\nu}(\underline{v}')$$

$$+ \frac{(1+\chi)}{2\varsigma kc} \imath \overline{\mathcal{L}^{s-\nu}(\underline{v}, \underline{y}_{\underline{\xi}_c}(\underline{v}'))} f_{k,\underline{\alpha},\nu}(\underline{v}') \Big\}, \quad \underline{v} \in U, \quad s = 1,2,\cdots, \tag{3.9b}$$

and $d_{2,k,\underline{\alpha},s}(\underline{v})$, $\underline{v}\in U$ can be obtained by arguing, as above, to obtain (3.9b). To approximate the systems of integral equations (3.7a), (3.7b) using (sparse) systems of linear equations, we use a family of wavelet bases introduced in [6]. Let $L^2(U)$ and $L^2(U')$ be the real Hilbert spaces of the square integrable functions defined on U and U', respectively, and let $M \geq 1$, $N \geq 2$ be integers, $\eta_i \in (0,1)$, $i=1,2,\cdots,N-1$, be $N-1$ points such that $\eta_i < \eta_{i+1}$, $i=1,2,\cdots,N-2$, and let $\underline{\eta}^N = (\eta_1,\eta_2,\cdots,\eta_{N-1})^T \in \mathbb{R}^{N-1}$. Moreover, we denote with $\mathcal{W}^M_{N,\underline{\eta}^N}(U')$ and $\mathcal{W}^M_{N,\underline{\eta}^N}(U)$, respectively, the orthonormal wavelet bases of $L^2(U')$ and $L^2(U)$ constructed in [6]. In particular, let us introduce the sets of indices $\mathcal{I}_{M,N,m}$, $m = 0,1,\cdots$, needed to represent the unknowns $c_{k,\underline{\alpha},s}$, $f_{k,\underline{\alpha},s}$, $s=0,1,\cdots$, of the system of integral equations (3.7a), (3.7b) in the basis $\mathcal{W}^M_{N,\underline{\eta}^N}(U')$ of $L^2(U')$. The data $d_{1,k,\underline{\alpha},s}$, $d_{2,k,\underline{\alpha},s}$, $s=0,1,\cdots$, of the system of integral equations (3.7a), (3.7b) is represented in the basis $\mathcal{W}^M_{N,\underline{\eta}^N}(U)$ of $L^2(U)$. That is, let us define

$$\mathcal{I}_{M,N,m} = \left\{ \underline{\mu} = (j,\hat{m},\nu)^T \,\middle|\, j = -M, -M+1, \cdots, M(N-1)-2, M(N-1)-1; \right.$$
$$\left. \hat{m} = \left\{ \begin{array}{ll} m, & j \geq 0, \\ 0, & j < 0, \end{array} \right. \quad \nu = 0,1,\cdots,(N^{\hat{m}}-1)_+ \right\}, \quad m = 0,1,\cdots. \tag{3.10}$$

We denote by $Y^M_{\underline{\mu},\underline{\mu}',N,\underline{\eta}^N}$ and by $\tilde{Y}^M_{\underline{\mu},\underline{\mu}',N,\underline{\eta}^N}$, $\underline{\mu},\underline{\mu}' \in \mathcal{I}_{M,N,m'}$, $m' = 0,1,\cdots$, respectively, the elements of the wavelet basis $\mathcal{W}^M_{N,\underline{\eta}^N}(U)$ and the wavelet basis $\mathcal{W}^M_{N,\underline{\eta}^N}(U')$, given in [6]. The following formulae hold (see [6] for further details):

$$K_{\xi_r,\xi_c}(\underline{v},\underline{v}') = \sum_{n=0}^{+\infty} \sum_{\underline{\mu}\in\mathcal{I}_{M,N,n}} \sum_{n'=0}^{+\infty} \sum_{\underline{\mu}'\in\mathcal{I}_{M,N,n'}} Y^M_{\underline{\mu},\underline{\mu}',N,\underline{\eta}^N}(\underline{v})$$
$$\sum_{m=0}^{+\infty} \sum_{\underline{\tilde{\mu}}\in\mathcal{I}_{M,N,m}} \sum_{m'=0}^{+\infty} \sum_{\underline{\tilde{\mu}}'\in\mathcal{I}_{M,N,m'}} \tilde{a}_{k,s,\underline{\mu},\underline{\mu}',\underline{\tilde{\mu}},\underline{\tilde{\mu}}'} \tilde{Y}^M_{\underline{\tilde{\mu}},\underline{\tilde{\mu}}',N,\underline{\eta}^N}(\underline{v}'), \quad \underline{v}\in U, \ \underline{v}'\in U', \tag{3.11a}$$

$$(1+\chi)\Phi(\underline{x}_{\xi}(\underline{v}),\underline{x}_{\xi_c}(\underline{v}')) = \sum_{n=0}^{+\infty} \sum_{\underline{\mu}\in\mathcal{I}_{M,N,n}} \sum_{n'=0}^{+\infty} \sum_{\underline{\mu}'\in\mathcal{I}_{M,N,n'}} Y^M_{\underline{\mu},\underline{\mu}',N,\underline{\eta}^N}(\underline{v})$$
$$\sum_{m=0}^{+\infty} \sum_{\underline{\tilde{\mu}}\in\mathcal{I}_{M,N,m}} \sum_{m'=0}^{+\infty} \sum_{\underline{\tilde{\mu}}'\in\mathcal{I}_{M,N,m'}} \hat{a}_{k,s,\underline{\mu},\underline{\mu}',\underline{\tilde{\mu}},\underline{\tilde{\mu}}'} \tilde{Y}^M_{\underline{\tilde{\mu}},\underline{\tilde{\mu}}',N,\underline{\eta}^N}(\underline{v}'), \quad \underline{v}\in U, \ \underline{v}'\in U', \tag{3.11b}$$

$$c_{k,\underline{\alpha},s}(\underline{v}') = \sum_{m=0}^{+\infty} \sum_{\underline{\mu}\in\mathcal{I}_{M,N,m}} \sum_{m'=0}^{+\infty} \sum_{\underline{\mu}'\in\mathcal{I}_{M,N,m'}} c_{k,\underline{\alpha},s,\underline{\mu},\underline{\mu}'} \tilde{Y}^M_{\underline{\mu},\underline{\mu}',N,\underline{\eta}^N}(\underline{v}'), \quad \underline{v}'\in U', \ s=0,1,\cdots, \tag{3.11c}$$

and formulae similar to formula (3.11c) hold for $f_{k,\underline{\alpha},s}(\underline{v}')$, $\underline{v}' \in U$, $d_{i,k,\underline{\alpha},s}(\underline{v})$, $\underline{v}\in U'$, $i=1,2$, $s=0,1,\cdots$. Let m^* be a positive integer. To approximate the system of integral equations (3.7a), (3.7b) using a system of finitely many linear equations, we truncate the sums in m and m' according to $m=m'=m^*$, in (3.11a)-(3.11c). The number of wavelet basis elements remaining in the series of the unknowns and of the data considered (see, for example, (3.11c)) after this truncation is $J_{M,N,m^*} = (M \cdot N^{m^*+1})^2$ (see [6,14]). Substituting these truncated wavelet expansions in (3.7a), (3.7b), we approximate the sequence of systems of

integral equations (3.7a), (3.7b) using the following sequence of systems of (complex) linear equations:

$$A^{k,M}\underline{v}^{k,\underline{\alpha},s,M}=\underline{d}^{k,\underline{\alpha},s,M}, \qquad s=0,1,\cdots, \tag{3.12}$$

where $\underline{v}^{k,\underline{\alpha},s,M}$, $\underline{d}^{k,\underline{\alpha},s,M}\in\mathbb{C}^{2J_{M,N,m^*}}$, $s=0,1,\cdots$, are finite dimensional (complex) vectors partitioned in J_{M,N,m^*} two-dimensional blocks. The two entries of each block of $\underline{v}^{k,\underline{\alpha},s,M}$ are, respectively, approximations of the coefficients of the wavelet expansion of the unknowns $c_{k,\underline{\alpha},s}$ and $f_{k,\underline{\alpha},s}$, $s=0,1,\cdots$. Similarly, the two entries of the two-dimensional blocks of $\underline{d}^{k,\underline{\alpha},s,M}$ are, respectively, approximations of the coefficients of the wavelet expansion of the data $d_{i,k,\underline{\alpha},s}$, $i=1,2$, $s=0,1,\cdots$. Let us assume for simplicity that the index i corresponds to the two indices $\underline{\mu}$, $\underline{\mu}'$ and the index j corresponds to the two indices $\underline{\tilde{\mu}}$, $\underline{\tilde{\mu}}'$. The matrix $A^{k,M}\in\mathbb{C}^{2J_{M,N,m^*}\times 2J_{M,N,m^*}}$ is a block partitioned matrix, the blocks of which are $(A_B^{k,M})_{i,j}$, $i,j=1,2,\cdots,J_{M,N,m^*}$. The blocks $(A_B^{k,M})_{i,j}$, $i,j=1,2,\cdots,J_{M,N,m^*}$, are 2×2 complex matrices. These blocks and the blocks of the vectors $\underline{v}^{k,\underline{\alpha},s,M}$, $\underline{d}^{k,\underline{\alpha},s,M}$ are ordered appropriately to yield (3.12) for application of the standard row by column matrix-vector multiplication rule (see [6] for further details). The 2×2 block $(A_B^{k,M})_{i,j}$ is defined as follows:

$$(A_B^{k,M})_{i,j}=\begin{pmatrix} \tilde{a}_{k,\underline{\alpha},s,\underline{\mu},\underline{\mu}',\underline{\tilde{\mu}},\underline{\tilde{\mu}}'} & \frac{1}{2\varsigma kc}\overline{\imath\hat{a}_{k,\underline{\alpha},s,\underline{\mu},\underline{\mu}',\underline{\tilde{\mu}},\underline{\tilde{\mu}}'}} \\ -\frac{2\lambda}{kc}\imath\hat{a}_{k,\underline{\alpha},s,\underline{\mu},\underline{\mu}',\underline{\tilde{\mu}},\underline{\tilde{\mu}}'} & \mu\tilde{a}_{k,\underline{\alpha},s,\underline{\mu},\underline{\mu}',\underline{\tilde{\mu}},\underline{\tilde{\mu}}'} \end{pmatrix}, \quad i,j=1,2,\cdots,J_{M,N,m^*}. \tag{3.13}$$

It is easy to see that when $k>0$, each block (3.13) is invertible if at least one of the entries is nonzero. The linear systems (3.12) are "dense" linear systems, that is, in general, all elements of the matrix $A^{k,M}$ are nonzero. However, due to the properties of the wavelet bases (see [6]), several coefficients of the wavelet expansions of the kernels (3.11a), (3.11b) (i.e., several "matrix elements" $(A_B^{k,M})_{i,j}$ of $A^{k,M}$) are "small". This fact suggests the use of a "sparse" approximation, $A^{k,M,\tau}=((A_B^{k,M,\tau})_{i,j})$, $i,j=1,2,\cdots,J_{M,N,m^*}$, of $A^{k,M}$, obtained by substituting zero for those elements of $A^{k,M}$ that are "smaller" than a (given) truncation threshold $\tau>0$. Using this truncation procedure, we approximate the solution to the dense linear system (3.12) as the solution to the sparse linear system

$$A^{k,M,\tau}\underline{v}^{k,\underline{\alpha},s,M}=\underline{d}^{k,\underline{\alpha},s,M}, \qquad s=0,1,\cdots, \tag{3.14}$$

the coefficients of which matrix, $A^{k,M,\tau}=((A_B^{k,M,\tau})_{i,j})\in\mathbb{C}^{2J_{M,N,m^*}\times 2J_{M,N,m^*}}$, $i,j=1,2,\cdots,J_{M,N,m^*}$, are defined as

$$(A_B^{k,M,\tau})_{i,j}=\begin{cases} (A_B^{k,M})_{i,j}, & \text{if } |||(A_B^{k,M})_{i,j}|||>\tau, \\ 0, & \text{if } |||(A_B^{k,M})_{i,j}|||\leq\tau, \end{cases} \quad i,j=1,2,\cdots,J_{M,N,m^*}, \tag{3.15}$$

where

$$|||(A_B^{k,M})_{i,j}|||=\sqrt{|\hat{a}_{k,s,\underline{\mu},\underline{\mu}',\underline{\tilde{\mu}},\underline{\tilde{\mu}}'}|^2+|\tilde{a}_{k,s,\underline{\mu},\underline{\mu}',\underline{\tilde{\mu}},\underline{\tilde{\mu}}'}|^2}, \qquad i,j=1,2,\cdots,J_{M,N,m^*}.$$

We transform the complex system (3.14) into an equivalent real system. We denote by $A^{r,k,M,\tau} \in \mathbb{R}^{4J_{M,N,m^*} \times 4J_{M,N,m^*}}$ the real matrix obtained by $A^{k,M,\tau}$ from the transformation of the 2×2 complex blocks $(A_B^{k,M,\tau})_{i,j}$, $i,j = 1,2,\cdots,J_{M,N,m^*}$, into 4×4 real blocks $(A_B^{r,k,M,\tau})_{i,j}$, i, $j = 1,2,\cdots,J_{M,N,m^*}$. Note that the complex systems (3.14) are transformed into $N_S \times N_S$ real systems, where $N_S = 4J_{M,N,m^*}$. Let $S > 0$ be an integer. We obtain an approximate solution to the problem (2.7a)-(2.7d) by solving the systems of integral equations (3.7a), (3.7b), using the method described previously for $s = 0,1,\cdots,S$. We compute an approximate value for the series given in (3.5a), (3.5b), truncated at $s = S$. We conclude this Section by explaining how to proceed, given the knowledge of the approximate solutions to the problems (2.7a)-(2.7d) considered to the corresponding approximate acoustic scattering cross section defined in (2.12). Given $k \in \mathbb{R}$, $k \neq 0$, it is easy to see that the following expansion holds:

$$\Phi_k(r\underline{\hat{x}},\underline{y}) = \frac{e^{ik\|r\underline{\hat{x}} - \underline{y}\|}}{4\pi\|r\underline{\hat{x}} - \underline{y}\|} = \frac{e^{ikr}}{4\pi r}\left(e^{-ik(\underline{\hat{x}}\cdot\underline{y})} + \mathcal{O}\left(\frac{1}{r}\right)\right), \quad \underline{y} \in \partial\Omega_c, \quad \underline{\hat{x}} \in \partial B, \quad r \to +\infty. \quad (3.16)$$

Substituting formula (3.16) in (3.5a) and using formula (2.9), we obtain

$$F_{\lambda,\mu}^0(\underline{\hat{x}},k,\underline{\alpha}) = \frac{1}{4\pi}\int_{U'}d\underline{v}'e^{-ik(\underline{\hat{x}}\cdot\underline{y}_{\xi_c}(\underline{v}'))}g_c(\underline{v}')c_{k,\underline{\alpha}}(\underline{y}_{\xi_c}(\underline{v}'))$$

$$= \frac{1}{4\pi}\int_{U'}d\underline{v}'e^{-ik(\underline{\hat{x}}\cdot\underline{y}_{\xi_c}(\underline{v}'))}g_c(\underline{v}')\sum_{s=0}^{+\infty}c_{k,\underline{\alpha},s}(\underline{v}'), \quad \underline{\hat{x}}, \underline{\alpha} \in \partial B. \quad (3.17)$$

Moreover, substituting (3.17) into (2.10), yields

$$C_{\lambda,\mu}(\underline{\hat{x}},k) = \frac{1}{4\pi}\int_{\partial B}\left|\int_{U'}d\underline{v}'e^{-ik(\underline{\hat{x}}\cdot\underline{y}_{\xi_c}(\underline{v}'))}g_c(\underline{v}')\sum_{s=0}^{+\infty}c_{k,\underline{\alpha},s}(\underline{v}')\right|^2 ds_{\partial B}(\underline{\alpha}), \quad \underline{\hat{x}} \in \partial B. \quad (3.18)$$

Formula (3.18) may be approximated by formula (2.12), that is, we approximate $C_{\lambda,\mu}$ with $\tilde{C}_{\lambda,\mu}$ given by

$$\tilde{C}_{\lambda,\mu}(\underline{\hat{x}},k) = \frac{1}{4\pi}\sum_{i=1}^{M_\theta-2}\sin(\theta_i^M)\sum_{j=0}^{M_\phi-1}\left|\int_{U'}d\underline{v}'e^{-ik(\underline{\hat{x}}\cdot\underline{y}_{\xi_c}(\underline{v}'))}g_c(\underline{v}')\sum_{s=0}^{+\infty}c_{k,\underline{\alpha}_{i,j},s}(\underline{v}')\right|^2, \quad \underline{\hat{x}} \in \partial B. \quad (3.19)$$

Finally, truncating the series expansion contained in (3.19) at order $s = S$ and the series expansions of $c_{k,\underline{\alpha}_{i,j},s}$, $i = 1,2,\cdots,M_\theta-2$, $j = 0,1,\cdots,M_\phi-1$ contained in (3.11c) at $m = m' = m^*$, we approximate (3.19) using the following formula:

$$\tilde{C}_{\lambda,\mu,S,M,N,m^*}^a(\underline{\hat{x}},k) = \frac{1}{4\pi}\sum_{i=1}^{M_\theta-2}\sin(\theta_i^M)\cdot\sum_{j=0}^{M_\phi-1}\left|\int_{U'}d\underline{v}'e^{-ik(\underline{\hat{x}}\cdot\underline{y}_{\xi_c}(\underline{v}'))}g_c(\underline{v}')\right.$$

$$\left.\left[\sum_{m=0}^{m^*}\sum_{\underline{\mu}\in\mathcal{I}_{M,N,m}}\sum_{m'=0}^{m^*}\sum_{\underline{\mu}'\in\mathcal{I}_{M,N,m'}}\sum_{s=0}^{S}c_{k,\underline{\alpha}_{i,j},s,\underline{\mu},\underline{\mu}'}\tilde{Y}_{\underline{\mu},\underline{\mu}',N,\underline{\eta}^N}^M(\underline{v}')\right]\right|^2, \quad \underline{\hat{x}} \in \partial B. \quad (3.20)$$

Formula (3.20) is the formula used to compute the approximate acoustic scattering cross sections shown in Section 5.

4   Parallel implementation

We now describe the parallel computation of the approximation of the acoustic cross section $\tilde{C}^a_{\lambda,\mu,S,M,N,m^*}(\underline{\hat{x}},k)$, defined in (3.20) for $\underline{\hat{x}} \in S_{N_\theta,N_\phi}$. Given the values of the parameters k, λ, μ, S, M, N, and m^*, the numerical method proposed to evaluate (3.20) is divided into two parts. That is,

1. For $\underline{\alpha} \in I_{M_\theta,M_\phi}$, compute the wavelet coefficients $c_{k,\underline{\alpha},s,\underline{\mu},\underline{\mu}'}$, $s = 0,1,\cdots,S$, $\underline{\mu} \in \mathcal{I}_{M,N,m}$, $\underline{\mu}' \in \mathcal{I}_{M,N,m'}$, $m,m' = 0,1,\cdots,m^*$, defined in (3.11c). This corresponds to the solution, using the method described in Section 3, to $M_{tot} = (M_\theta - 2) \cdot M_\phi + 2$ time-harmonic scattering problems (2.7a)-(2.7d);

2. For $\underline{\hat{x}} \in S_{N_\theta,N_\phi}$, compute $\tilde{C}^a_{\lambda,\mu,S,M,N,m^*}(\underline{\hat{x}},k)$ given in (3.20).

Note that because the parallel implementation of Part 1 has already been presented in [14], it is only summarized here for the convenience of the reader. The first level of parallelism in the execution of Part 1 of the computation (see Fig. 2) arises from the fact that, for a given value of the parameters λ and k, we must solve M_{tot} exterior boundary value problems (2.7a)-(2.7d). In fact, these exterior boundary value problems are independent of one another. We associate a value of the index ν to each of these problems, that is, we use $\nu = 1,2,\cdots,M_{tot}$. The polar angles corresponding to the propagation direction of the incoming wave associated with the ν-th problem are chosen as follows: For $\nu = 1$: $\theta_1^{*,M} = \phi_1^{*,M} = 0$; For $\nu = 2,3,\cdots,M_{tot}-1$: $\theta_\nu^{*,M} = \theta_{1+int((\nu-2)/M_\phi)}^M$, $\phi_\nu^{*,M} = \phi_{(\nu-2)-M_\phi int((\nu-2)/M_\phi)}$; Finally, for $\nu = M_{tot}$: $\theta_{M_{tot}}^{*,M} = \pi$, $\phi_{M_{tot}}^{*,M} = 0$, where $int(\cdot)$ is the integer part of $\cdot$. Let N_p, N_g be two positive integers. For simplicity, suppose that we have at our disposal $N_g \cdot N_p$ processors. We divide these processors into N_g groups of N_p processors. Denote by $p_{j,i}$ the i-th processor of the j-th group, $i = 1,2,\cdots,N_p$, $j = 1,2,\cdots,N_g$. Choose the first processor of each group to be the master processor of the processors of its group, that is, we have N_g group masters $p_{j,1}$, $j = 1,2,\cdots,N_g$. Moreover, when necessary, the processor $p_{1,1}$ will act as master of the group masters. To keep the exposition simple, we approximate the system of integral equations (3.7a), (3.7b), using a vector space generated by $J_{M,N,m^*} = N_p^q$ wavelet basis functions, where q is a positive integer greater than or equal to one. Finally, we assume, for simplicity, that M_{tot}/N_g is an integer.

The first level of parallelism is exploited by assigning, for $j = 1,2,\cdots,N_g-1$, and to the j-th group of processors, the solution to the problems (2.7a)-(2.7d) indexed by $\nu = 1+(j-1)M_{tot}/N_g$, $2+(j-1)M_{tot}/N_g,\cdots,jM_{tot}/N_g$. To the processors of the group $j = N_g$ are assigned the solution to the problems indexed by $\nu = 1+(N_g-1)M_{tot}/N_g$, $2+(N_g-1)M_{tot}/N_g,\cdots,M_{tot}$ (see, for further details, [14]). A second level of parallelism in the execution of *Part* 1 of the computation is contained in the solution to each problem (2.7a)-(2.7d). This level of parallelism is exploited inside each of the N_g groups of N_p processors (see Fig. 2). There are two tasks in the second level of parallelism: computation of the elements of the $J_{M,N,m^*} \times J_{M,N,m^*}$ coefficient matrix mentioned above (this computation is carried out once by the processors of each group) and, for each choice of $\theta_\nu^{*,M}$, $\phi_\nu^{*,M}$,
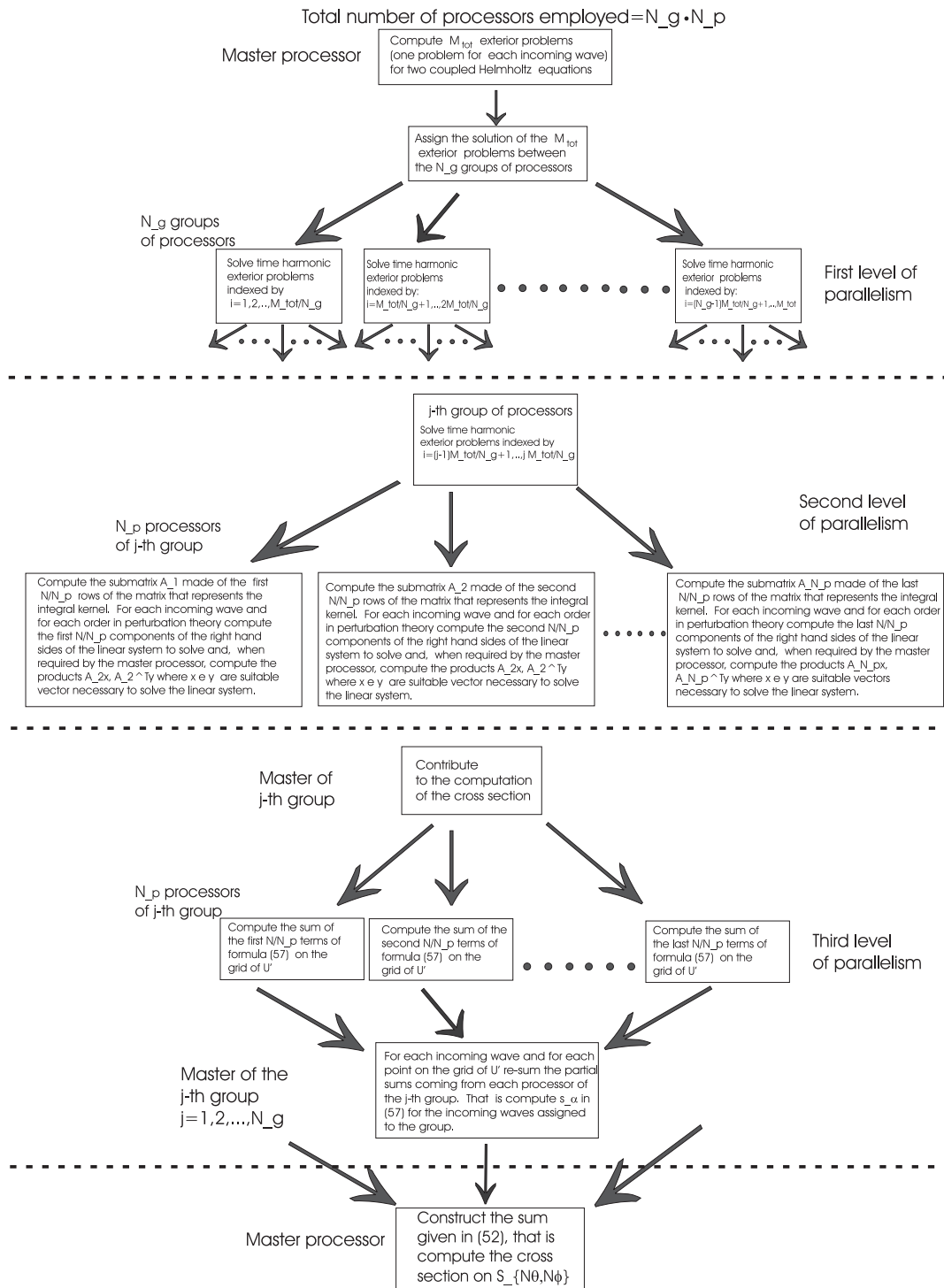
Total number of processors employed=N_g ∙N_p

Master processor

Compute M_{tot} exterior problems (one problem for each incoming wave) for two coupled Helmholtz equations

Assign the solution of the M_{tot} exterior problems between the N_g groups of processors

N_g groups of processors

Solve time harmonic exterior problems indexed by: i=1,2,..,M_tot/N_g

Solve time harmonic exterior problems indexed by: i=M_tot/N_g+1...,2M_tot/N_g

Solve time harmonic exterior problems indexed by: i=(N_g-1)M_tot/N_g+1...M_tot

First level of parallelism

j-th group of processors

Solve time harmonic exterior problems indexed by i=(j-1)M_tot/N_g+1,...,j M_tot/N_g

Second level of parallelism

N_p processors of j-th group

Compute the submatrix A_1 made of the first N/N_p rows of the matrix that represents the integral kernel. For each incoming wave and for each order in perturbation theory compute the first N/N_p components of the right hand sides of the linear system to solve and, when required by the master processor, compute the products A_2x, A_2^Ty where x e y are suitable vector necessary to solve the linear system.

Compute the submatrix A_2 made of the second N/N_p rows of the matrix that represents the integral kernel. For each incoming wave and for each order in perturbation theory compute the second N/N_p components of the right hand sides of the linear system to solve and, when required by the master processor, compute the products A_2x, A_2^Ty where x e y are suitable vector necessary to solve the linear system.

Compute the submatrix A_N_p made of the last N/N_p rows of the matrix that represents the integral kernel. For each incoming wave and for each order in perturbation theory compute the last N/N_p components of the right hand sides of the linear system to solve and, when required by the master processor, compute the products A_N_px, A_N_p^Ty where x e y are suitable vectors necessary to solve the linear system.

Master of j-th group

Contribute to the computation of the cross section

N_p processors of j-th group

Compute the sum of the first N/N_p terms of formula (57) on the grid of U'

Compute the sum of the second N/N_p terms of formula (57) on the grid of U'

Compute the sum of the last N/N_p terms of formula (57) on the grid of U'

Third level of parallelism

Master of the j-th group j=1,2,...,N_g

For each incoming wave and for each point on the grid of U' re-sum the partial sums coming from each processor of the j-th group. That is compute s_α in (57) for the incoming waves assigned to the group.

Master processor

Construct the sum given in (52), that is compute the cross section on S_{Nθ,Nφ}

Figure 2: The three levels of parallelism.

$\nu=1,2,\cdots,M_{tot}$, computation of the right hand sides of the linear systems (3.14). The matrix coefficients smaller than a given threshold τ ($\tau > 0$) are discarded according to formula (3.15), and, hence, they are not stored. The fact that each processor has only a portion of the matrix to compute and that the matrix has several elements approximated by zero makes possible the computation and storage of matrices of very high dimension using limited resources. Indeed, because each processor usually has a certain amount of memory at its disposal, the larger the number of processors used to perform this computation, the larger the dimension of the matrix that can be stored.

Next, the N_p processors belonging to a group are used to compute the (truncated) wavelet expansion of the right hand sides of the systems of integral equations (3.7a), (3.7b), that is, the right hand sides of the linear systems (3.14), which must be solved by the group of processors considered. For each right hand side considered, this computation consists of the numerical evaluation of J_{M,N,m^*} complex double integrals. These integrals are independent of each other and are computed in parallel. In this phase of the computation, some work must be replicated in exchange for removing the need for communication between the processors in each group and between the different groups of processors. When the processors belonging to a group have computed the coefficients of the wavelet expansion of the right hand side of a linear system (3.14), they communicate their results to the master processor of the group, which begins computation of the solution to the linear system using an ad hoc parallel implementation of the conjugate gradient method. The master processor of a group uses the N_p processors of its group to solve the linear systems. In the execution of the conjugate gradient method, the processors belonging to a group are used in parallel to compute the (row by column) product of the coefficient matrix of the linear system with its transposed matrix. An iteration of the conjugate gradient method is completed when each processor of the group communicates its results, obtained by performing these products, to the master processor of the group (see [14] for further details). Finally, we discuss the parallel implementation of Part 2 of the computation, that is, the computation of $\tilde{C}^a_{\lambda,\mu,S,M,N,m^*}(\hat{\underline{x}},k)$ for $\hat{\underline{x}} \in S_{N_\theta,N_\phi}$ (see (3.20)). This involves a third level of parallelism (see Fig. 2).

Note that computation of formula (3.20) requires the numerical approximation of the following integral:

$$a(\hat{\underline{x}},\underline{\alpha}) = \int_{U'} d\underline{v}' e^{-ik(\hat{\underline{x}}\underline{y}_{\xi_c}(\underline{v}'))} g_c(\underline{v}')$$

$$\Big[\sum_{m=0}^{m^*} \sum_{\underline{\mu} \in \mathcal{I}_{M,N,m}} \sum_{m'=0}^{m^*} \sum_{\underline{\mu}' \in \mathcal{I}_{M,N,m'}} \sum_{s=0}^{S} c_{k,\underline{\alpha},s,\underline{\mu},\underline{\mu}'} \tilde{Y}^M_{\underline{\mu},\underline{\mu}',N,\underline{\eta}^N}(\underline{v}') \Big], \quad \hat{\underline{x}} \in S_{N_\theta,N_\phi}, \quad \underline{\alpha} \in I_{M_\theta,M_\phi}. \quad (4.1)$$

Let R_u be a positive integer that denotes the number of quadrature nodes in U' used to approximate the integral in (4.1). Let $\underline{v}'_l$, p_l, $l=1,2,\cdots,R_u$ be the nodes and the weights of the quadrature rule used. Note that to compute (4.1), it is convenient to sum the wavelet coefficients on the grid I_{M_θ,M_ϕ} and on the R_u quadrature nodes, that is, it is convenient to

compute the following functions:

$$s_{\underline{\alpha}}(\underline{v}') = \sum_{m=0}^{m^*} \sum_{\underline{\mu} \in \mathcal{I}_{M,N,m}} \sum_{m'=0}^{m^*} \sum_{\underline{\mu}' \in \mathcal{I}_{M,N,m'}} \tilde{Y}^M_{\underline{\mu},\underline{\mu}',N,\underline{\eta}^N}(\underline{v}') \left(\sum_{s=0}^{S} c_{k,\underline{\alpha},s,\underline{\mu},\underline{\mu}'} \right), \quad \underline{v}' \in U', \ \underline{\alpha} \in I_{M_\theta,M_\phi}, \quad (4.2)$$

on the quadratures nodes of U', store the result obtained, and sum the addenda of (3.20) as follows:

$$\tilde{C}^a_{\lambda,\mu,S,M,N,m^*}(\hat{\underline{x}},k) = \frac{1}{4\pi} \sum_{i=1}^{M_\theta-2} \sin(\theta_i^M) \sum_{j=0}^{M_\phi-1} \left| \sum_{l=1}^{R_u} p_l e^{-ik(\hat{\underline{x}},\underline{y}_{\tilde{\xi}_c}(\underline{v}'_l))} g_c(\underline{v}'_l) s_{\underline{\alpha}_{i,j}}(\underline{v}'_l) \right|^2, \quad \hat{\underline{x}} \in \partial B. \quad (4.3)$$

The cost of computing (4.3) is $R_u \cdot ((M_\theta-2) \cdot M_\phi) \cdot ((N_\theta-2) \cdot N_\phi+2) + R_u \cdot ((M_\theta-2) \cdot M_\phi) \cdot J_{M,N,m^*}$ elementary operations. In fact, $R_u \cdot ((M_\theta-2) \cdot M_\phi) \cdot J_{M,N,m^*}$ elementary operations are necessary to approximate the function $s_{\underline{\alpha}}(\underline{v}')$ on the quadrature nodes of U' for $\underline{\alpha} \in I_{M_\theta,M_\phi}$. To this cost, we must add the cost of re-summing the appropriate expressions containing $s_{\underline{\alpha}}(\underline{v}')$ on the R_u quadrature nodes of U' for $\hat{\underline{x}} \in S_{N_\theta,N_\phi}$, given by $R_u \cdot ((M_\theta-2) \cdot M_\phi) \cdot ((N_\theta-2) \cdot N_\phi+2)$ elementary operations. That is, the parallel procedure has a computational cost for each group of processors of $R_u \cdot ((M_\theta-2) \cdot M_\phi)/N_g) \cdot (J_{M,N,m^*}/N_p) + R_u \cdot (((M_\theta-2) \cdot M_\phi)/N_g) \cdot ((N_\theta-2) \cdot N_\phi+2)/N_p$ elementary operations.

5   A case study: the acoustic scattering cross section of the simplified NASA space shuttle

In the numerical experiments presented in this Section, we computationally modeled several acoustic scattering cross section conditions for a furtive simplified model of the NASA space shuttle using formulae (2.12) and (3.20). The original model of the NASA space shuttle (see Fig. 1(b)) was modified (see Fig. 1(a)) to allow representation (3.1) of its boundary, using, as the cylindrical axis, the "symmetry" axis of the main body of the shuttle. The data relative to the original obstacle (see Fig. 1(b)) may be downloaded from the website: `http://www.nasa.gov/multimedia/3d_resources/assets/sts.html`. The physical dimensions of the shuttle are expressed in *units* such that $1 unit = 56.14/14 meters$. The maximum length of the shuttle in the direction of the symmetry axis of its main body is $14 units$. The space shuttle is an acoustically hard obstacle, that is, we have $\chi = +\infty$, and the speed of sound in air is assumed to be $c = 331.45 meters/seconds$, which corresponds approximately to $c = 82.65 units/seconds$. The surfaces ξ_r, ξ_c were chosen such that the kernels K_{ξ_r,ξ_c} and $\Phi(\underline{x}_{\xi_r}, \underline{y}_{\xi_c})$ were continuous with respect to their first partial derivatives. These surfaces ξ_r, ξ_c were obtained by smoothing the surface ξ and implementing a kind of magnification along the symmetry axis of the smoothed ξ. The wavelength of the time-harmonic incoming waves was 0.2 *units*, which corresponded to a wave number $k = 10\pi \ units^{-1}$. These parameters resulted in a ratio between the characteristic length of the obstacle ($14 units$) and the wavelength of the incoming waves ($0.2 units$) of seventy.

To numerically solve the time-harmonic scattering problems (2.7a)-(2.7d) needed to compute the cross sections shown in Figs. 3-7, we chose $M=1$, $N=4$, $m^*=3$, $S=1$. With these choices, each scattering problem is approximated by a square complex linear systems with a coefficient matrix composed of $J_{M,N,m^*}=(M\cdot N^{m^*+1})^2=2^{16}=65536$ two by two blocks (see (3.14)), corresponding to square linear systems of (real) dimension $N_S=4J_{M,N,m^*}=262144$. Moreover, we chose $\tau=5\times10^{-4}$. The incoming wave propagation directions used to approximate the acoustic scattering cross section were the directions contained in the set I_{M_θ,M_ϕ} defined in (2.11b), for $M_\theta=6$, $M_\phi=12$. The set S_{N_θ,N_ϕ}, corresponding to the observation directions of the scattered field and of the acoustic cross section, was the set defined in (2.11a) for $N_\theta=12$, $N_\phi=24$. In the computation, the cross section the origin of the spherical coordinate system was taken to be the same as that used to represent the boundary of the obstacle in cylindrical coordinates (the center of mass of the obstacle). The symmetries of the obstacle were exploited in the computation. Let us first show the effect of the smart strategy in reducing the entire solid angle of the acoustic cross section. In the following, to avoid confusion, we denote the spherical coordinates by (r,θ,ϕ_s) and the cylindrical coordinates by (r_1,ϕ,x_3). Recall that these two coordinate systems have the same origin, and that we chose $\phi=\phi_s$.

Fig. 3 shows the surface $\xi(x_3,\phi)$, $x_3\in[-7,7]$, $\phi\in[0,2\pi)$ of the simplified version of the NASA space shuttle (a), the acoustic cross section $C_{\lambda,\mu}$ (multiplied by 40) (measured in $unit^2\,Kg^2/sec^4$) of the passive obstacle (b), and the acoustic cross section $C_{\lambda,\mu}$ (multiplied by 40) (measured in $unit^2\,Kg^2/sec^4$) of the smart obstacle for $\lambda=0.5$ (c). Recall that the cross section is a function of $\underline{\hat{x}}=\underline{\hat{x}}(\theta,\phi_s)$, $\theta\in[0,\pi]$, $\phi\in[0,2\pi)$, and note that in Fig. 3, the cross section is represented in cylindrical coordinates. In fact, in Fig. 3, the cross sections are represented as follows: to $\underline{\hat{x}}$, we associate (θ,ϕ_s), and to (θ,ϕ_s), we associate $x_3=7\cos(\theta)$, $\phi=\phi_s$, $\theta\in[0,\pi]$, $\phi_s\in[0,2\pi)$. In this way, we represent the cross section in cylindrical coordinates using the surface of a cylinder of radius 9, and the cylindrical axis given by the x_3 axis is zero for $x_3\in[-7,7]$ and $\phi\in[0,2\pi)$ (Fig. 3). Visualization of the cross section assists an understanding of the relation between the features of the obstacle and the peaks of the cross section. We see that the cross section of the passive obstacle is sensibly larger than the cross section of the smart obstacle ($\lambda=0.5$). Moreover, the two cross sections take their maxima according to the largest extension of the "wings", $x_3\approx6$, $\phi=0,\pi,2\pi$ and of the "vertical stabilizer", $x_3\approx6.5$ and $\phi=3\pi/2$, of the shuttle.

Fig. 4 shows, from left to right, the acoustic cross sections (multiplied by 80) of the passive obstacle and of the smart obstacle ($\lambda=0.5$). The cross sections are represented in the radial coordinates of the spherical coordinate system using the surface of a sphere of radius 9, such that the center is at the origin as zero. This last surface is chosen as zero because the sphere of radius 9, with the center at the origin, can contain the obstacle. The view of the obstacle and its cross section, as shown in Fig. 4, together assist an understanding of the scattering phenomenon studied. Note that the smart strategy, with $\lambda=0.5$, satisfactorily reduces the scattered field on almost the entire solid angle, except for the part of the solid angle corresponding to the "wings" of the obstacle located approximately at $\phi_s=0$, π, 2π, $\theta=\pi/9$ (i.e., $x_1\in(-5,5)$, $x_2=0$ and $x_3\in(4,6)$) and to the
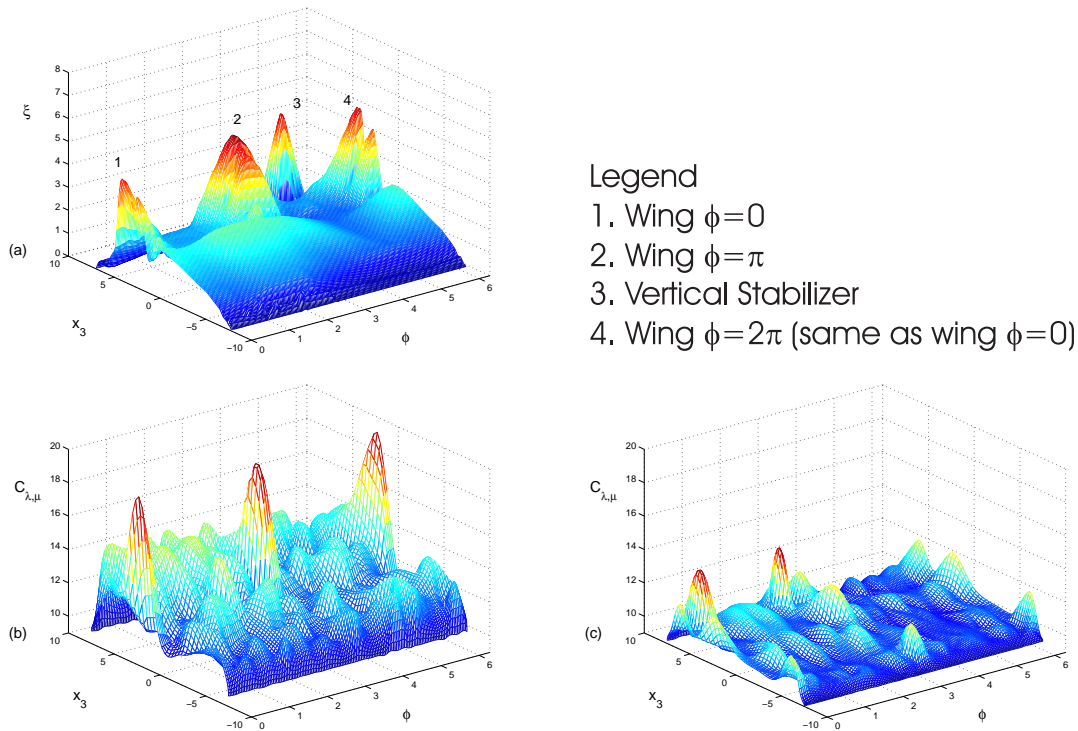
Figure 3: Furtivity effect: (a) boundary of the obstacle ξ, (b) cross section of the passive obstacle $C_{\lambda,\mu}$ (multiplied by 40), (c) cross section of the smart obstacle ($\lambda = 0.5$) $C_{\lambda,\mu}$ (multiplied by 40).
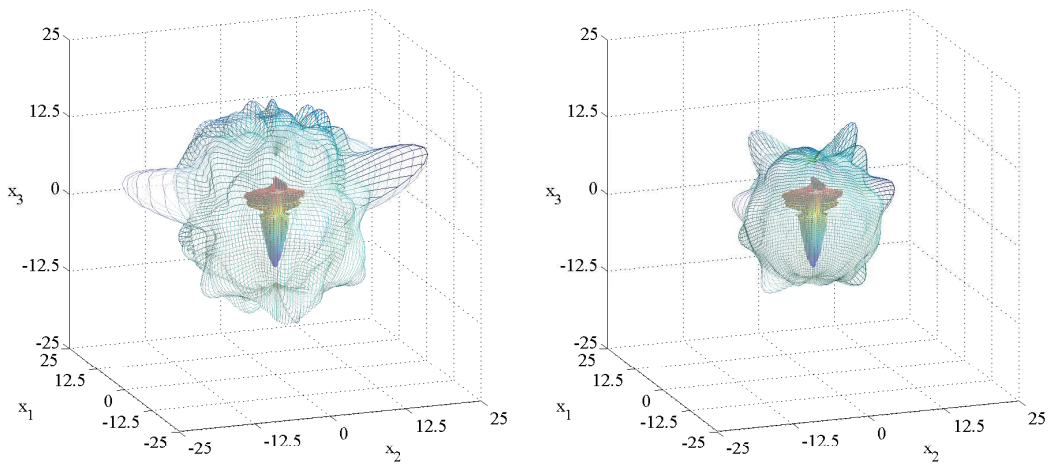

Figure 4: From left to right, the acoustic cross section ($unit^2 \, Kg^2/sec^4$) of the passive obstacle (multiplied by 80) and of the smart obstacle ($\lambda = 0.5$) (multiplied by 80) represented in the radial coordinate using the surface of a sphere of radius 9, and assigning the center of the sphere to the origin, to represent a value of zero for the cross section. Inside this sphere is shown a model of the obstacle positioned coherently within the cross section.

vertical stabilizer, located approximately at $\phi_s = 3\pi/2$, $\theta = \pi/9$ (i.e., $x_1 = 0$, $x_2 \in (1,4)$, $x_3 \in (6,7)$). We want to examine the relation between the smart strategy and the scattered field by studying the magnitude of the coefficients of the series expansions appearing in (3.5a), (3.5b). Recall that we have chosen $S = 1$. We consider the following quantities:

$$m_{c,k,\underline{\alpha}}^{\lambda} = \frac{1}{2J_{N,M,m^*}} \sum_{s=0}^{1} \sum_{m=0}^{m^*} \sum_{\underline{\mu} \in \mathcal{I}_{M,N,m}} \sum_{m'=0}^{m^*} \sum_{\underline{\mu}' \in \mathcal{I}_{M,N,m'}} |c_{k,\underline{\alpha},s,\underline{\mu},\underline{\mu}'}^{\lambda}|, \qquad \alpha \in \partial B, \ \lambda \in [0,1], \qquad (5.1a)$$

$$m_{f,k,\underline{\alpha}}^{\lambda} = \frac{1}{2J_{N,M,m^*}} \sum_{s=0}^{1} \sum_{m=0}^{m^*} \sum_{\underline{\mu} \in \mathcal{I}_{M,N,m}} \sum_{m'=0}^{m^*} \sum_{\underline{\mu}' \in \mathcal{I}_{M,N,m'}} |f_{k,\underline{\alpha},s,\underline{\mu},\underline{\mu}'}^{\lambda}|, \qquad \alpha \in \partial B, \ \lambda \in [0,1], \qquad (5.1b)$$

and we consider the ratio

$$r_{c,k,\underline{\alpha}}^{\lambda} = \frac{m_{c,k,\underline{\alpha}}^{\lambda}}{m_{c,k,\underline{\alpha}}^{0}}, \quad \underline{\alpha} \in \partial B, \quad \lambda \in [0,1], \qquad (5.2)$$

and the quantities

$$r_{c,k}^{\lambda} = \frac{1}{M_\theta M_\phi} \sum_{i=1}^{M_\theta} \sum_{j=1}^{M_\phi} r_{c,k,\underline{\alpha}_{i,j}}^{\lambda}, \qquad \lambda \in [0,1], \qquad (5.3a)$$

$$r_{f,k}^{\lambda} = \frac{1}{M_\theta M_\phi} \sum_{i=1}^{M_\theta} \sum_{j=1}^{M_\phi} m_{f,k,\underline{\alpha}_{i,j}}^{\lambda}, \qquad \lambda \in [0,1], \qquad (5.3b)$$

where $\underline{\alpha}_{i,j} = \alpha(\theta_i^M, \phi_j^M) = (\sin\theta_i^M \cos\phi_j^M, \sin\theta_i^M \sin\phi_j^M, \cos\theta_i^M)^T$, $i = 1,2,\cdots,M_\theta$, $j = 1,2,\cdots,M_\phi$, see (2.12). The quantity $r_{c,k}^{\lambda}$ is a measure of the mean reduction of the wavelet coefficient amplitudes of the acoustic scattered fields as a function of $\lambda \in [0,1]$, and the quantity $r_{f,k}^{\lambda}$ is a measure of the mean cost of the smart strategy measured in terms of the amplitudes of the wavelet coefficients of the pressure current as a function of $\lambda \in [0,1]$.

Table 1 shows the quantities $r_{c,k}^{\lambda}$, $r_{f,k}^{\lambda}$, for $\lambda = 0.5$, $\lambda = 1 - 10^{-6}$, and the ratio $r_{c,k,\underline{\alpha}}^{\lambda}$ given in (5.2) for the same values of λ and for some incoming directions $\underline{\alpha}(\theta, \phi_s) \in I_{M_\theta, M_\phi}$. The

Table 1: Furtivity effect on the wavelet coefficients.

$(\theta, \phi_s) \in I_{M_\theta, M_\phi}$	$r_{c,k}^{0.5}$	$r_{c,k,\underline{\alpha}}^{1-10^{-6}}$	$m_{f,k,\underline{\alpha}}^{0.5}$	$m_{f,k,\underline{\alpha}}^{1-10^{-6}}$
$(\pi/5, 0)$	0.739	0.533	2.06×10^{-5}	2.11×10^{-3}
$(\pi/5, \pi)$	0.813	0.237	5.51×10^{-6}	8.43×10^{-4}
$(3\pi/5, 0)$	0.562	0.472	2.14×10^{-5}	9.89×10^{-4}
$(3\pi/5, \pi/2)$	1.01	0.216	3.01×10^{-5}	9.61×10^{-6}
$(3\pi/5, \pi)$	0.813	0.237	4.96×10^{-6}	1.11×10^{-2}
$(4\pi/5, 0)$	0.658	0.685	3.26×10^{-5}	1.74×10^{-3}
mean value on I_{M_θ, M_ϕ}	$r_{c,k}^{0.5} = 0.442$	$r_{c,k}^{1-10^{-6}} = 0.319$	$r_{f,k}^{0.5} = 9.55 \times 10^{-6}$	$r_{f,k}^{1-10^{-6}} = 5.56 \times 10^{-4}$

furtivity effect induced by the pressure current reduces, on average, the amplitudes of the wavelet coefficients of the acoustic scattered fields by about 55.8% (i.e., $1-0.442=0.558$) for $\lambda=0.5$, and by about 68.1% (i.e., $1-0.319=0.681$) for $\lambda=1-10^{-6}$. Note that, as shown in Table 1, the improvement in the furtivity effect obtained in going from $\lambda=0.5$ to $\lambda=1-10^{-6}$ implies a cost associated with the "size" of the pressure current used to obtain the furtivity effect, measured by $r_{f,k}^{\lambda}$. Furthermore, Table 1 shows that for some incoming directions of the incident wave, the smart strategy fails to hide the obstacle. In particular, these critical directions are those along which the scattering effects of some of the features of the obstacle are relevant (that is, the effects of the "wings" corresponding to (θ,ϕ_s) equal to $(\pi/5,0)$, $(3\pi/5,\pi)$, of the "vertical stabilizer" corresponding to $(\theta,\phi_s)=(3\pi/5,3\pi/2)$, or of the prow corresponding to $(\theta,\phi_s)=(4\pi/5,0)$).

Let us examine, in detail, some of these incoming directions. For example, let us consider the direction $\hat{\underline{\alpha}}=(\sin(4\pi/5)\cos(5\pi/3),\sin(4\pi/5)\sin(5\pi/3),\cos(4\pi/5))$, that is, a direction along which the effects of the prow are relevant. We select this direction of incoming wave to complete the analysis of the scattering cross section shown in Figs. 3 and 4. In fact, these figures do not clearly show the effects of the prow. In particular, in Fig. 5, the (θ,ϕ_s) plane is shown on the color scale alongside the modulus of the far field, $F_{\lambda,\mu}^0(\hat{\underline{x}}(\theta,\phi_s),k,\hat{\underline{\alpha}})$ (multiplied by 9) for $\lambda=0,0.5,1-10^{-6}$. The corresponding cross sections $C_{\lambda,\mu}(\hat{\underline{x}}(\theta,\phi_s),k)$ (multiplied by 9) are shown in Fig. 6. Figs. 5, 6 are presented in the same color scale. Fig. 5 shows that the far fields of the passive obstacle and the smart obstacle, for $\lambda=0.5$, reveal the presence of the wings and prow. That is, the far field corresponding to the smart obstacle, for $\lambda=0.5$, behaves similarly to the far field corresponding to the passive obstacle. In contrast, the behavior of the far field corresponding to the smart obstacle, for $\lambda=1-10^{-6}$, is satisfactory. This effect depends on the incoming wave propagation direction considered. In fact, the acoustic cross section (see Fig. 6) shows that the smart strategy works well for $\lambda=0.5$. Finally, Fig. 7 shows that along the direction $(\theta,\phi_s)=(4\pi/5,\pi/30)$, the scattered field is large. This is probably due to the effects of the wings and prow. However, Fig. 7 shows also that along this direction, the smart strategy works satisfactorily for the two values of λ considered. Finally, Figs. 5, 6, 7 show that the vertical stabilizer is the element of the obstacle that is the most difficult to make furtive. Instead, the prow is the element of the obstacle that the smart strategy hides satisfactorily. The website `http://www.ceri.uniroma1.it/ceri/zirilli/w7` contains virtual reality and stereographic applications related to the acoustic scattering cross sections of the simplified NASA space shuttle.
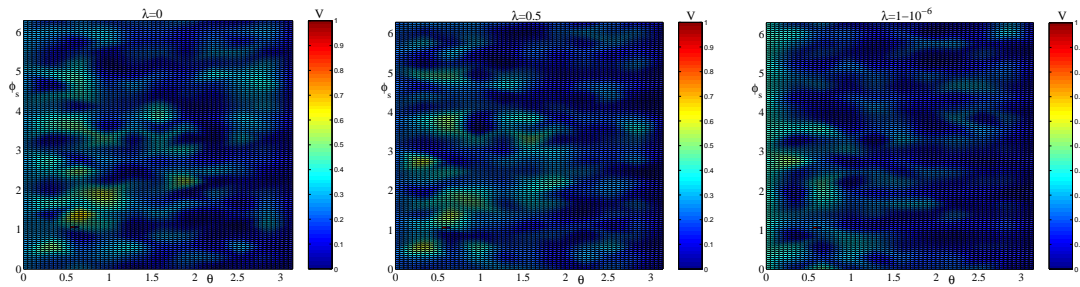

Acknowledgments

Figure 5: From left to right, the modulus of the far field $F^0_{\lambda,\mu}(\hat{\underline{x}}(\theta,\phi_s),k,\underline{\alpha})$ multiplied by 9 (i.e., $V = 9|F^0_{\lambda,\mu}(\hat{\underline{x}}(\theta,\phi_s),k,\underline{\alpha})|$) for $\underline{\alpha} = (\sin(4\pi/5)\cos(5\pi/3),\sin(4\pi/5)\sin(5\pi/3),\cos(4\pi/5))$, plotted on the (θ,ϕ_s) plane of the passive obstacle and of the smart obstacle, for $\lambda = 0.5$ and $\lambda = 1-10^{-6}$.
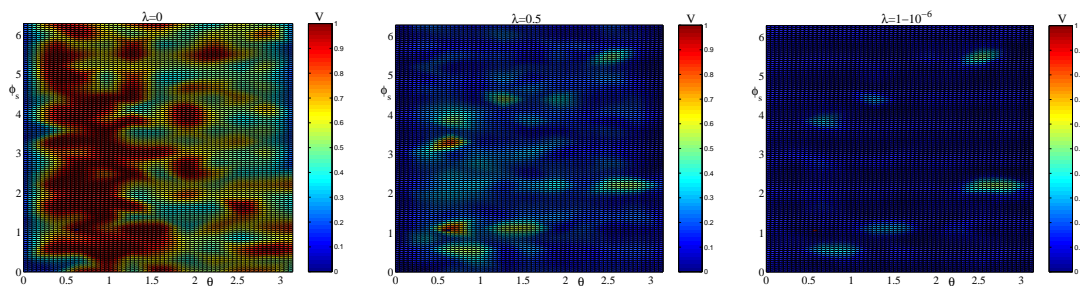

Figure 6: From left to right, the modulus of the acoustic cross section multiplied by 9 (i.e., $V = 9C_{\lambda,\mu}(\hat{\underline{x}}(\theta,\phi_s),k)$), plotted on the (θ,ϕ_s) plane of the passive obstacle and of the smart obstacle, for $\lambda = 0.5$ and $\lambda = 1-10^{-6}$.
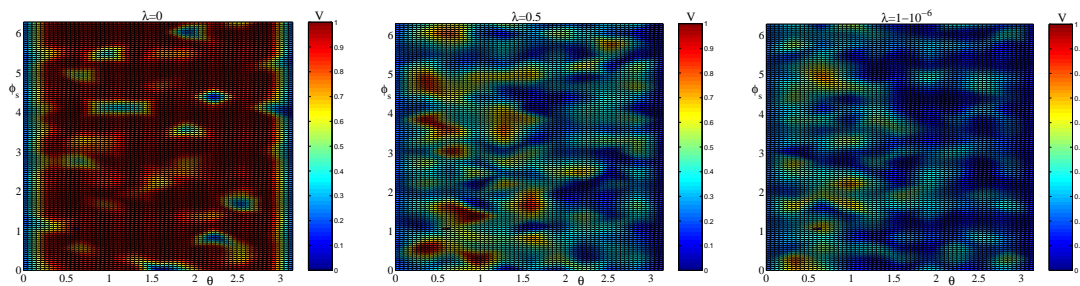

Figure 7: From left to right, the modulus of the far field $F^0_{\lambda,\mu}(\hat{\underline{x}}(\theta,\phi_s),k,\underline{\alpha})$ multiplied by 9 (i.e., $V = 9|F^0_{\lambda,\mu}(\hat{\underline{x}}(\theta,\phi_s),k,\underline{\alpha})|$) for $\underline{\alpha} = (\sin(4\pi/5)\cos(\pi/3),\sin(4\pi/5)\sin(\pi/3),\cos(4\pi/5))$, plotted on the (θ,ϕ_s) plane of the passive obstacle and of the smart obstacle, for $\lambda = 0.5$ and $\lambda = 1-10^{-6}$.

References

[1] B. Chambers, A smart radar absorber, J. Smart. Mater. Struct., 8 (1999), 64–72.

[2] B. Chambers and K. L. Ford, A smart microwave absorber, IEE Electr. Lett., 36 (2000), 50–52.

[3] B. Chambers and A. Tennant, General analysis of the phase-switched screen part 1: the single layer case, Proceedings IEE part F-Radar Sonar Navigation, 149 (2002), 243–247.

[4] B. Chambers and A. Tennant, Influence of switching waveform characteristics on the performance of a single layer phase-switched, IEEE T. Electromagn. C., 44 (2002), 434–441.

[5] L. Fatone, G. Pacelli, M. C. Recchioni and F. Zirilli, Optimal-control methods to study two new classes of smart obstacles in time-dependent acoustic scattering, J. Eng. Math., 56 (2006), 385–413.

[6] L. Fatone, G. Rao, M. C. Recchioni and F. Zirilli, High performance algorithms based on a new wavelet expansion for time dependent acoustic obstacle scattering, Commun. Comput. Phys., 2 (2007), 1139–1173.

[7] L. Fatone, M. C. Recchioni and F. Zirilli, A numerical method to solve an acoustic inverse scattering problem involving ghost obstacles, J. Inverse. Ill-Posed. Prob., 15 (2007), 57–82.

[8] L. Fatone, M. C. Recchioni and F. Zirilli, A method to solve an acoustic inverse scattering problem involving smart obstacles, Waves. Random. Complex., 16 (2006), 433–455.

[9] L. Fatone, M. C. Recchioni and F. Zirilli, A masking problem in time dependent acoustic obstacle scattering, Acoust. Res. Lett. Onl., 5(2) (2004), 25–30.

[10] L. Fatone, M. C. Recchioni and F. Zirilli, Furtivity and masking problems in time dependent electromagnetic obstacle scattering, J. Opt. Theory. Appl., 121 (2004), 223–257.

[11] L. Fatone, M. C. Recchioni and F. Zirilli, A parallel numerical method to solve high frequency ghost obstacle acoustic scattering problems, J. Appl. Comput. Electromagn. Soc., 23 (2008), 220–232.

[12] I. Foster, C. Kesselman and S. Tuecke, The anatomy of the grid, Int. J. Supercomput. Appl., 15(3) (2001), 200–222.

[13] F. Mariani, M. C. Recchioni and F. Zirilli, The use of the Pontryagin maximum principle in a furtivity problem in time-dependent acoustic obstacle scattering, Waves. Random. Complex., 11 (2001), 549–575.

[14] S. Migliori, G. Bracco, L. Fatone, M. C. Recchioni and F. Zirilli, A parallel code for time dependent acoustic scattering involving passive or smart obstacles, Int. J. High Perform. Comput. Appl., 25(1) (2011), 70–92.

[15] A. G. Ramm, Invisible obstacles, Ann. Pol. Math., 90 (2007), 145–148.